An indirect, negative radiative effect of water vapor in the tropics and its implications for regional surface heat stress

Jaya Khanna[1] and Karan karan[1]

[1]National Institute of Science Education and Research

October 27, 2023

Abstract

We report an indirect, negative, cloud-mediated, surface radiative effect (RE) of water vapor (IWVE) in certain regions in the tropics, which may be consequential for day-to-day regional heat stress. Using reanalysis and satellite data we show that this effect is marked by a surprisingly dominant positive relationship of cloud RE with near surface and column humidity. These clouds are predominantly low level and altocumuli, previously reported to have a negative surface RE, possibly lending the net negative RE to water vapor. Also reported earlier, these clouds form in the mid-troposphere, as detrainment offshoots of deep convective towers and can be advected away to large distances, hence requiring no local convective triggering in the IWVE regions. Evidently, the IWVE are co-located with the horizontal branch of the Hadley cell, with the lowest vertical forcing in the tropics. Moreover, these are also the transition regions between the highly cloudy and the driest parts of the tropics, with a waning down occurrence of cirrus, deep convective and altostratus clouds, linked with positive RE, corroborating the hypothesis. IWVE regions also show a large temporal variability in humidity possibly providing opportunity for a large variability in cloud fractional coverage, however the mechanism controlling this covariability is not understood. The IWVE is tightly tied with the seasonal cycle of the ITCZ and hence is likely a dominant source of pre-monsoon surface temperature variability and heat stress in the current climate. The evolution of the IWVE under future climate warming needs further investigation.

An indirect, negative radiative effect of water vapor in the tropics and its implications for regional surface heat stress

J. Khanna[1,2], Karan[1,2]

[1]School of Earth and Planetary Sciences, National Institute of Science Education and Research, Jatni, 752050, India
[2]Homi Bhabha National Institute, Training School Complex, Anushaktinagar, Mumbai, 400094, India

Key Points:

- An indirect, water vapor related surface cooling is observed at the daily scale, pan-tropics, bordering the ITCZ, throughout the year
- Lower tropospheric humidity is negatively related with local cloud radiative forcing in these regions dominated by mid level clouds
- Regions occur along the horizontal branch of Hadley cell, move with the seasonal cycle, possibly consequential for pre-monsoon heat stress

Corresponding author: Jaya Khanna, `jkhanna@niser.ac.in`

Abstract

We report an indirect, negative, cloud-mediated, surface radiative effect (RE) of water vapor (IWVE) in certain regions in the tropics, which may be consequential for day-to-day regional heat stress. Using reanalysis and satellite data we show that this effect is marked by a surprisingly dominant positive relationship of cloud RE with near surface and column humidity. These clouds are predominantly low level and altocumuli, previously reported to have a negative surface RE, possibly lending the net negative RE to water vapor. Also reported earlier, these clouds form in the mid-troposphere, as detrainment offshoots of deep convective towers and can be advected away to large distances, hence requiring no local convective triggering in the IWVE regions. Evidently, the IWVE are co-located with the horizontal branch of the Hadley cell, with the lowest vertical forcing in the tropics. Moreover, these are also the transition regions between the highly cloudy and the driest parts of the tropics, with a waning down occurrence of cirrus, deep convective and altostratus clouds, linked with positive RE, corroborating the hypothesis. IWVE regions also show a large temporal variability in humidity possibly providing opportunity for a large variability in cloud fractional coverage, however the mechanism controlling this covariability is not understood. The IWVE is tightly tied with the seasonal cycle of the ITCZ and hence is likely a dominant source of pre-monsoon surface temperature variability and heat stress in the current climate. The evolution of the IWVE under future climate warming needs further investigation.

Plain Language Summary

The greenhouse radiative effect of water vapor on surface temperatures is widely known. However, can water vapor cause an 'apparent' radiative cooling effect under certain conditions? Here, we show that in certain extensive tropical regions, bordering the ITCZ, the lower tropospheric water vapor has a substantial relation with cloud occurrence, which subsequently renders an indirect surface cooling effect in high humidity conditions. These clouds are majorly shallow and mid level cumuli, which are known to have a negative surface radiative forcing. What causes the positive relation between lower tropospheric humidity and these clouds, is not understood. However, that these regions border the ITCZ and hence are co-located with the horizontal branch of the Hadley cell, suggests low amounts of convective triggering and hence high level clouds. The potentially reduced warming from the high level clouds may give the lower level clouds an upper hand in the net radiative impact. Lastly, these regions precede the ITCZ in time as they move north-south with it. This may be consequential for pre-monsoonal heat stress in tropical regions.

1 Introduction

Water vapor is frequently dubbed as the most important greenhouse gas which plays a dominant role in climate change through the water vapor feedback (Soden et al., 2002, 2005; Forster et al., 2021; Dessler et al., 2013). This control is delivered through the dominant impact of the increase in the upper tropospheric humidity on trapping the outgoing longwave radiation (OLR) and recycling it within the climate system (Soden et al., 2005; Allan et al., 1999; Dessler et al., 2013). This trapping of energy warms up all components of the climate system - the atmosphere, land and oceans. However, on hourly to daily time scales, it is the near surface humidity (or column integrated water vapor, as they are strongly correlated) which dominates the greenhouse effect of water vapor as manifested at the land surface (Shakespeare & Roderick, 2021; Flerchinger et al., 2009; M. Li et al., 2018; Brutsaert, 1975; Carmona et al., 2014). Idealized modeling studies of clear sky surface downwelling longwave radiation (DLR) are able to explain about 97% of the temporal variability in DLR with near surface humidity (q_{sfc}) and surface temperatures (T_{sfc}) (Shakespeare & Roderick, 2021). High positive correlations have been reported between in-situ observed q_{sfc} and DLR (or T_{sfc}), at daily to monthly time scales, in all sky conditions (Gaffen et al., 1992; Ross et al., 2002; M. Li et al., 2018). However, exceptions to this behavior (Ross et al., 2002), relatively understudied, highlight the role of the several other complex climatic processes that water vapor involves itself in - surface evapotranspiration, cloud formation, convective amplification etc - in impacting T_{sfc}. The resulting processes may modulate the initial water vapor greenhouse effect at regional scales. We set out to investigate this regionality in the 'effective' water vapor greenhouse effect, particularly in the tropics, and investigate the role of clouds in causing the exceptional behavior.

This study is motivated by the need to understand the regionality in the q_{sfc}-T_{sfc} relationship, to better analyse the recent increase in global heat stress (Alizadeh et al., 2022; Pai et al., 2013; Mazdiyasni et al., 2017; X. X. Li, 2020; D. Li et al., 2020), which is predicted to increase to deadly levels in tropical latitudes under climate change, especially in transition regions like the Sahel, the Cerrado and southern Asia (Coffel et al., 2018; Mahlstein et al., 2011; Coumou et al., 2013; Hoegh-Guldberg et al., 2018) affecting low income communities and ecosystems of these regions (Alizadeh et al., 2022; Dunne et al., 2013). Over the Amazon-Cerrado boundary in Brazil, trees are reported to be close to their threshold temperature for photosynthesis, already impacting these ecosystems during high heat stress conditions (Araújo et al., 2021; Tiwari et al., 2021; Reich et al., 2015). Over the densely populated southern Asia, pre-monsoon heat stress has emerged as a major challenge under climate change (Rohini et al., 2016; Pai et al., 2013). These regions are additionally impacted by the combined effects of high temperature and humidity on perceived heat, corroborating the challenge even further (Oldenborgh et al., 2018; Wehner et al., 2016; Im et al., 2017). This surmounting evidence raises the need to understand the impact of near surface humidity on surface temperatures and the covariability between them.

Over and above the impact of near surface humidity on DLR, discussed above, q_{sfc} can impact T_{sfc} through other processes that control surface warming. For example, it is suggested that evaporative cooling from intense irrigation, which will probably result in a negative correlation between the two variables, can cause a muted local warming of the surface (Oldenborgh et al., 2018; Lobell & Bonfils, 2008; Lobell et al., 2008; Puma & Cook, 2010; Douglas et al., 2009; Lawston et al., 2020). However, this process is applicable to regional scales only, where a substantial amount of irrigation is practiced, which is expected only in a small part of the tropics. Additionally, this process takes effect only in the dry season of the region when precipitation is low (Biemans et al., 2016; Douglas et al., 2006). Hence, a large spatial and temporal scale impact is not expected from this mode of surface cooling, especially not in the pre-monsoon season, when agriculture is anyways low due to the low supply of riverine or ground waters for irrigation, and high heat stress conditions (Biemans et al., 2016).

Lower tropospheric humidity is also crucial in cloud formation and hence can potentially influence CRF at regional scales, a relationship which we set out to investigate in this study. As an example of the former relationship, q_{sfc} plays the lead role in convective triggering, supporting conditions conducive to moist convection by reducing convective inhibition - a higher near surface moisture has been shown to have a positive impact on moist convection and cumulus clouds (Findell & Eltahir, 2003a, 2003b). Free tropospheric humidity above the boundary layer is also shown to support moist convection by reducing the detrainment drying of convective plumes (Derbyshire et al., 2004; de Rooy et al., 2013; Holloway et al., 2009; Schiro et al., 2016). However, such positive impact of q_{sfc} on cloud formation could be marred by other complex processes like prevailing atmospheric stability and horizontal advection, which may interfere with the relation between these variables in regions outside the tropical deep convection belt. In other words, humidity-cloud relationships may or may not be the same as the above for non-convective clouds. In this study, we show the existence of extended regions in the tropics where q_{sfc} and CWV are dominantly, positively correlated with shallow to mid tropospheric clouds which are reported, by previous studies, to have a negative surface radiative forcing (Bourgeois et al., 2016; Bouniol et al., 2012; Riihimaki et al., 2012; Stein et al., 2011; Parker et al., 2016). These regions thereby show an 'effective', net negative radiative impact of q_{sfc} (CWV) on T_{sfc} on a daily scale, specifically in the pre-monsoon season when heat stress is at its highest at these latitudes.

Hence, this study focuses on understanding the impact of q_{sfc}, through its relation with local cloud cover, on daily scale surface heat stress in tropical regions during the peak, pre-monsoon, summer season. The general correlations between the humidity and surface temperature variables are presented first, subsequently relating the observation to the local cloud cover and variability. Next, the relationship of these correlations with the larger scale atmospheric dynamics is presented. Lastly, a short analysis is presented to propose a possible role of the near surface humidity in causing observed heat stress through the processes identified.

2 Methods

This study focuses on processes that impact the daily scale variability of regional surface temperatures (T_{sfc}). As such, most analysis uses daily scale data for a selected month. This choice of time scales reflects our interest in the 'instantaneous' response of T_{sfc} to the radiative forcing by the variability in water vapor and clouds. Since the latter process takes of the order of a few hours to manifest, the day-to-day co-variability in the variables is analyzed, if not the co-variability at sub-daily time scales. The atmospheric water vapor variability at longer time scales might itself be caused by inter-seasonal and inter-annual climate variability and climate change, but that is not the focus of this study. However, our analysis with inter-annual, monthly averaged variables results in similar inferences as the analysis with daily scale variables, providing support for the generalizability of the processes identified. Results are majorly reported from the pre-monsoon summer season of the northern hemisphere, but the inferences remain unchanged for other seasons. The month of May 2016 is chosen for some specific analysis that is limited by the size of the data set involved. 2016 was a post El Niño year transitioning to a mild La Niña, infested by high heat stress in the Indian subcontinent (Oldenborgh et al., 2018).

Surface heat stress is quantified with daily scale maximum surface temperatures (T_{max}) from reanalysis and satellite datasets. T_{max} appears frequently and takes an important role in the formal estimation of heat stress (IMD, 2002; Perkins, 2015). However, in this study, heat stress is used to refer to periods of statistically significant departures of T_{max} from the climatological or monthly mean and should not be confused with the various heat wave indices used by meteorological departments to declare periods of heat stress. Most inferences reported here with T_{max} remain unchanged for an analysis with daily averaged surface temperatures (T_{avg}) and daily maximum 2 m air temperature ($T_{2m,max}$).

The daily averaged near surface specific humidity (q_{sfc}), specific humidity at various altitudinal levels (q_z) and total column water vapor (CWV) are used to capture the radiative effect of atmospheric water vapor on surface temperatures. Previous studies have utilized these variables to show that at daily to monthly timescales, in most global land areas these variables are non-linearly but positively correlated with the surface downwelling longwave radiation (DLR) or surface temperatures (Gaffen et al., 1992; Ross et al., 2002). Although the clear sky regression coefficients between q_{sfc} and DLR are space dependent (Allan et al., 1999), there is no previous evidence of them being negative. Hence, q_{sfc} is used to represent the greenhouse impact of atmospheric water vapor on surface temperatures (Shakespeare & Roderick, 2021).

ERA5 is the major source of daily and monthly average meteorological fields for the years 2001 to 2020 at a horizontal resolution of 0.25°×0.25° (Hersbach et al., 2020, 2023). Surface skin temperature and 1000 hPa specific humidity from the global analysis are used to represent T_{max} and q_{sfc} respectively. Supporting analysis is performed with Level 3 standard retrievals, version 7 from AIRS (AIRS, 2019) for the period 2001 to 2020 at a spatial resolution of 1°×1°. The daily daytime surface skin temperature from the ascending branch and daily near surface specific humidity averaged between the ascending (equator passing time - 1:30 pm LT) and descending (equator passing time - 1:30 am LT) branches are used to represent T_{max} and q_{sfc} respectively.

Cloud cover information is obtained from ERA5 at the same spatial resolution as that for T_{max} and q_{sfc}. Cloud fields are also obtained from CERES monthly average daytime cloud product, CldTypHist, for the period 2001 to 2020 at a spatial resolution of 1°×1° (Doelling et al., 2013, 2016). CERES CldTypHist characterizes clouds based on three altitude and three optical depth bins. The lowest level (1000 hPa to 680 hPa) has Cumulus, Stratocumulus and Stratus with optical depths 0.0-3.6, 3.6-23 and 23-380 respectively. The middle level (680 hPa to 440 hPa) has Altocumulus, Altostratus and Nimbostratus with optical depths 0.0-3.6, 3.6-23 and 23-380 respectively. The highest level (440 hPa to 10 hPa) have Cirrus, Cirrostratus and Deep Convective clouds with optical depths 0.0-3.6, 3.6-23 and 23-380 respectively. AIRS daily total cloud cover data is also used for the same analysis.

Surface cloud radiative forcing (CRF) is majorly estimated with hourly scale, daytime (6:00 am to 6:00 pm LT) surface radiative fluxes from ERA5. CERES SYN1deg level 3 product is also used to derive the daily scale CRF for May 2016 at a spatial resolution of 1°×1° (Doelling et al., 2013, 2016). The CRF is estimated as a difference between the all-sky and clear-sky net radiation at the surface (Ramanathan et al., 1989).

Most analysis in this work is performed using statistics like linear correlation coefficients, linear regressions coefficients and anomalies from spatio-temporal averages for daily scale data analyzed over a month. Statistical significance is obtained with a two-tailed t-test for correlation coefficients, linear regressions and differences at the 95% confidence level in all cases.

Some of the analysis is performed over the African subcontinent because the contiguous nature of this region across the equator into the two hemispheres provides the opportunity to investigate the processes studied along a meridian, without disruption from land-ocean boundaries and high topography. The generality of these processes, if applicable, over other continents is indicated by providing relevant details in the text.

Figures 1 and S1 show the multiyear mode of monthly correlations of daily scale T_{max} (or $T_{2m,max}$, T_{avg}) and q_{sfc} (or CWV). Multiyear mode is calculated using grid-scale monthly correlations for 20 years, from four neighboring grid points, regardless of the statistical significance of the correlations in individual years. However, the correlations of interest (IWVE correlations defined in 'Results and Discussion') are robustly significant across all years. Fig. S1b is shown as an example and will be discussed in detail in the next section.

3 Results and Discussion

The objective of this study is to identify regions where water vapor impacts surface heat stress through processes over and above its greenhouse warming impact. In other words, we endeavor to investigate regions where the direct greenhouse effect of water vapor may be masked by the radiative impacts of the other climatically important processes mediated by water vapor, like cloud formation. To identify such regions, a basic correlation analysis between daily scale surface temperature and indicators of atmospheric humidity is performed.

3.1 A negative correlation between near surface atmospheric water vapor and maximum daily surface temperatures

At the daily scale, T_{max} of a majority of regions around the globe are strongly positively correlated with q_{sfc} (Fig. 1), and CWV (Fig. S1 a) in ERA5 and also in AIRS (Fig. S2 a). The values of these correlation coefficients for May 2016, are displayed in Fig. S1 b to show that the spatial patterns of the multiyear mode of these correlations (Figs. 1, S1) compare well with the values for individual years. These widespread positive correlations could be attributed to the greenhouse effect of water vapor. The maximum positive correlations larger than ≈0.7 are obtained at high latitudes and moderate values over the tropical oceans, a feature of the surface temperature-humidity relationship reported before (Ross et al., 2002). The inhibition of these positive correlations along the inter-tropical convergence zone (ITCZ) over land could be attributable to the dominant presence of high level clouds in these regions, which may have a complex net CRF. The analysis of these regions is out of the scope of this study.

The same figures, however, also show several tropical and sub-tropical land regions with high, statistically significant, negative correlations between daily T_{max} and q_{sfc} which occur across seasons and the two data sets used. Such signal has previously been observed over western USA using radiosonde data (Ross et al., 2002). In our study the negative correlation coefficients range between -0.36 to -0.97 for data averaged for May between 2001 and 2020 (Fig. 1). The largest negative correlations are found predominantly over tropical Africa and tropical South America throughout the year and over the Indian subcontinent, southeast Asia and northern Australia in some seasons. Similar patterns appear also with T_{avg} and $T_{2m,max}$ (Figs. S1 c and S1 d) and with inter-annual correlations using monthly averaged data (Fig. S2 b), indicating the generalizability of this relationship. This apparent water vapor related cooling is observed over land areas on the flank regions of the ITCZ and follows its seasonal cycle (Fig. 1). Hence, for example over the Indian subcontinent, it comes into prominence in the dry, pre-monsoon summer season (Fig. S3). It should be noted however that these negative correlations might maximize in a region's peak monsoon period. This is probably due to an atmospheric moistening and a sharp evaporative surface cooling due to heavy precipitation - for example in June over India when the monsoons arrive over land (Fig. S3). However, the cause of the water vapor related cooling in the pre-monsoon dry period is not obvious.

This negative correlation of near surface water vapor with surface temperatures, suggesting an apparent negative radiative forcing from water vapor is termed here as the 'Indirect Water Vapor Effect' or IWVE. This apparent indirect forcing of water vapor is investigated next. In the following, IWVE correlations will mean a correlation between daily q_{sfc} and T_{max}, unless otherwise specified. Furthermore, the positive IWVE correlation regions over the deep convective regions near the equator are termed as the ITCZ and the positive IWVE correlation regions polewards of the IWVE regions are termed as the desert or DES regions.

Figure 2 shows the correlations between specific humidity at an altitude (q_z) and daily T_{max} over three regions of the African subcontinent - an IWVE, an ITCZ and a DES region in May 2016. These regions are carefully chosen to lie at the same longitude (19°E) and away from topography. Over the IWVE region, the correlation between T_{max} and q_z is always significantly negative throughout the troposphere. Similarly, over the DES region the above correlation is significantly positive throughout. However, over the ITCZ region the correlation is positive close to the surface but changes to negative in the upper half of the troposphere. The altitudinal dependence of the correlations over the ITCZ suggests a complex interplay of multiple processes, possibly involving clouds and water vapor, impacting surface temperatures, which is out of the scope of this study. Only the IWVE regions, where q_{sfc} dominates the overall correlation between CWV and T_{max}, are studied here. This is a reasonable choice because most IWVE regions defined based on Figures 1 and S1 also show a consistent negative correlation with CWV (Fig. 3).

3.2 IWVE regions occur between the cloudiest and clearest parts of the tropics

Figures 1, S1 and S2 also show an overlay of total cloud cover averaged over the indicated time periods from ERA5. The IWVE co-occurs with regions of transition cloud cover, tropics-wide, i.e. between regions of maximum and minimum cloud cover where its gradient is substantial. For example, during May over central Africa (Fig. 1 b), the average cloud cover over the IWVE regions is around 0.51 (standard deviation 0.17), as compared to around 0.71 (0.18) over the ITCZ and 0.24 (0.18) over the DES regions. Hence, the total cloud cover in the IWVE regions is intermediate between regions of predominant convection (ITCZ) and regions of predominant downwelling (over subtropical deserts like the Sahara, Kalahari, the Arabian desert etc). Additionally, the fact that the IWVE regions tightly border the equatorial regions of deep convection everywhere, and follow the north-south march of the ITCZ, suggests that the IWVE correlations could be mediated by the radiative effects of some specific clouds that are dominant at the borders of the ITCZ.

Next, a possible pathway, mediated by clouds, is analyzed, which may lead to the apparent negative radiative forcing from water vapor in the IWVE regions. These regions receive much lower precipitation than the ITCZ (Fig. S4) which suggests that the IWVE regions may harbor clouds, or a cloud distribution, that is distinctly different from those in the ITCZ, resulting in a distinctly different CRF. Clouds show a spectrum of surface and top of atmosphere CRF depending upon their cloud top height and optical depth (Chen et al., 2000; Hartmann et al., 1992). A radiative transfer calculation is often necessary to obtain the net radiative effect of a certain vertical distribution of clouds. However, in this study we have taken evidential support from previous research to tie the observed cloud distribution over the IWVE regions with the negative, apparently cloud-mediated radiative impact of q_{sfc}, both of which are discussed below. A comprehensive numerical analysis of these relationships is left for a follow up study.

3.3 IWVE regions are dominated by 'cooling' mid tropospheric clouds

Figure 4 shows the distribution of the daytime low, mid and high level clouds zonally averaged over a region in Africa (30°N, 17.5°E and 30°S, 30°E), obtained from the CERES CldTypHist product for May 2001 to 2020. The corresponding May average cloud maps for Africa are provided in Figure S5. There is a clear distinction in the distribution of different types of clouds between the ITCZ, IWVE and DES regions. The IWVE regions are marked by a dominant presence of low and mid level, optically thin to moderately thick clouds, like shallow cumuli, altocumuli and stratocumuli. While the ITCZ, apart from the low and mid level clouds, also have a higher percentage of optically thin to thick, mid and high clouds, relative to the IWVE regions. This feature is present in all seasons except when the IWVE correlations are large during the monsoon, apparently due to the presence of strong evaporative surface cooling (August in Northern Hemisphere in Figure 4c), in which case the low and altocumulus clouds become infrequent over the IWVE regions. Specifically, the non-monsoonal, IWVE regions show a dominant presence of mid level, low thickness altocumulus clouds, which follow the poleward boundaries of the IWVE regions and are present abundantly and uniformly between these latitudes (Figure S5 d).

The effective radiative impact of this disparate cloud distribution on surface temperatures over the IWVE, ITCZ and DES regions is expected to be different. Noticeably, low level shallow cumulus and mid level altocumulus and altostratus have been previously shown to have a negative radiative forcing on surface temperatures (Chen et al., 2000; Hartmann et al., 1992). Additionally, the predominant occurrence of thin (optical depth around 1.03) mid level clouds (3 to 8 km) with a possibly negative radiative forcing over land has been previously reported in the pre-monsoon months over western Africa in the Nigerian region (Bouniol et al., 2012; Bourgeois et al., 2016; Stein et al., 2011), in Darwin (Riihimaki et al., 2012) and in the pre-monsoon Indian subcontinent (Parker et al., 2016). These mid level, thin, altocumulus clouds with a negative radiative forcing in the tropical regions (Bourgeois et al., 2016), are associated with mid level detrainment from deep convective clouds near the zero degree isotherm (Johnson et al., 1996, 1999; Iwasa et al., 2012). It is suggested that the latent heat of condensation to ice causes the deep convective tower to lose buoyancy and form these clouds, which can get horizontally advected to far away regions. As such, the occurrence and radiative impact of such mid level clouds is likely to be important in the flank regions of the equatorial deep convective belt, which is where the IWVE regions occur.

Hence, the dominant shallow- and alto- cumulus clouds in the IWVE regions could be responsible for the observed surface cooling. However, the question - how is q_{sfc} in the IWVE regions linked to surface cooling caused through these clouds? - is still open. This is an important question, because the expected positive, greenhouse radiative forcing of water vapor seems to be negated by a mechanism that supports clouds with a negative radiative impact. This mechanism should cause the aforementioned cooling clouds to occur along with high q_{sfc} in the IWVE regions. Given the strength and robustness of the IWVE correlations over several time and spatial scales, this mechanism could have great significance for the heat stress dynamics in the IWVE regions. Although the exact mechanism is not investigated here, we show evidence of such a negative relationship between CRF and q_{sfc} that exists dominantly over the IWVE regions, rendering the 'effective' negative radiative forcing from water vapor.

Over the IWVE regions, we find a robust, significant and large negative (positive) regression between q_{sfc} and daytime CRF (cloud fractional coverage, figure not shown), but insignificant regression between these quantities in the DES regions and positive, insignificant values in some areas of the ITCZ (Fig. 5). This feature of the IWVE, ITCZ and DES regions is observed pan-tropics (Figures 6 and S6) throughout the year (figures not shown). However, we do find the ITCZ regions to have a significant negative correlation between upper tropospheric water vapor and CRF (figure not shown) indicating a dependence of cloud formation on local environmental humidity, as is presumably also the case over the IWVE regions. In the IWVE regions, we however find this strong dependence of CRF on the water vapor present throughout the column (figure not shown). In other words, in the IWVE regions, water vapor in the lower and higher tropospheric levels seems to vary and impact cloud cover in tandem. The mechanism behind this apparent correlation is not understood, however, the correlation enables lower tropospheric water content to be a good indicator of CRF in these regions.

Lastly, the IWVE regions also show a large day-to-day variability in both cloud cover and CRF, which is not present in the DES and ITCZ regions (Fig. 5). Over DES, q_{sfc} is too low to be associated with substantial cloud occurrence, whereas, over the ITCZ it is too high to limit or control the same. While we have not established any cause-and-effect relationships between q_{sfc} and cloud cover in the three regions, the general atmospheric conditions do seem to be less conducive to or supportive of clouds over the DES regions and vice versa over the ITCZ. Some of this possibly could be attributed to the stable conditions that form over the DES regions due to Hadley circulation and vice versa over the ITCZ. The IWVE regions however show a large variability in both q_{sfc} and CRF, suggesting atmospheric conditions variable enough to support different types and amounts of clouds. This feature is observed in most IWVE regions throughout the tropics (figure not shown). The effect of tropical latitudinal overturning circulation on the IWVE regions is analyzed next.

3.4 IWVE co-located with the horizontal branch of Hadley cell - cloudiness not dominated by convective forcing

Cloud formation or occurrence is governed by several factors like water availability and the presence of a vertical lift - either due to buoyancy, low level convergence, turbulence, orography or frontal interaction. As such, a weak control from one factor can give the other processes an upper hand in impacting cloud formation or occurrence. Specifically, the absence of one factor can result in a decrease in a certain type of clouds and favor the other types. The role of a presence or absence of vertical lift on cloud occurrence in the three regions will now be investigated.

An abundant amount of convective forcing is available over the ITCZ throughout the year due to maximum solar insolation, which results in the high cloud cover and precipitation associated with these regions discussed earlier. The divergence of the horizontal wind, column integrated between 500 hPa and 200 hPa in the tropics, shows positive values (divergence) over the ITCZ regions (Fig. 7). Hence, the regions where q_{sfc} is positively (not) correlated with T_{max} (CRF) are also the regions of deep convective forcing. The high cloud cover of all types in these regions supports this inference (Fig. 4). The opposite is true for DES regions which show predominant horizontal convergence, downwelling and clear skies (Fig. 7).

The IWVE regions, on the other hand, are marked by the smallest horizontal divergence and vertical motion as depicted in Figure 7. This is seen by the overlap between the IWVE regions and the contours of near zero divergence of the horizontal winds integrated over the upper troposphere. This feature is present over all IWVE regions in the tropics. This absence of a strong vertical forcing could be related with the dominance of shallow cumulus and altocumulus clouds and the lower areal coverage of deep convective and cirrus clouds in the IWVE regions (Figure 4). It can only be speculated now and verified in a numerical study that vertical forcing is conducive to a certain type of clouds, the absence of which may be related with the IWVE.

3.5 Why could the water vapor indirect effect be important?

The co-location of the IWVE regions with transition cloud cover and negligible vertical motion (or convective forcing) indicate that these regions occur in the horizontal branches of tropical continental scale overturning circulations like the Hadley cell. Clearly, the Hadley cell is not strictly meridionally oriented everywhere, which is why we don't find a strict latitudinal dependence of the IWVE regions over various continents in a given season. In fact, continental scale overturning circulations, like the one found over the northern Sahara in May 2016 (Figure 7), can also engender IWVE regions co-located with their horizontal branches. However, Figure 1 demonstrates clearly that the IWVE is not present in regions between Libya and Mali over a climatological average and may not be important for the regional heat stress climatology. However, in regions affected by a climatological latitudinal overturning circulation, like the Hadley cell, the IWVE could be decisive in determining pre-monsoonal surface heat stress.

To this effect, we provide an example of the surface heat stress during the severe, pan-India heat wave of May 2016. An exhaustive analysis of the general heat stress at these latitudes, their relation with the IWVE and any deviations will be presented in a follow up study. India lies in the Southeast Asian belt where both high temperature and high humidity contribute significantly to heat stress (Im et al., 2017; Hoegh-Guldberg et al., 2018; Wehner et al., 2016) particularly in April, May and June. While IWVE shows an inverse relationship between these variables, their combination could be above the extreme heat wave threshold, as shown by Wehner et al. (2016) for May 2015 in Hyderabad, India. Hence, this region has been chosen for a case study. Record high near surface temperatures of 51 degrees were observed in Phalodi, Rajasthan (27.13°N, 72.36°E) around 19^{th} May 2016 with the heat wave impacting regions pan-India between the months of April and June (Agarwal, 2016; Wu, 2016; Mazdiyasni et al., 2017; Oldenborgh et al., 2018). The impact of this heat wave on human health was severe as evidenced by a high number of newspaper reports on heat strokes and human fatalities in this period (Tharoor, 2016). We present a preliminary meteorological analysis of this heat wave to show a possible relevance of the IWVE during the heat wave period.

Sources of tropical heat stress are not as well understood as are for their extra-tropical counterparts (Perkins, 2015). For example, there are only a handful of studies which apply the 'blocking high' theory of heat waves to these latitudes (Rohini et al., 2016; Ratnam et al., 2016; Oueslati et al., 2017). We endeavor to show through this analysis that the IWVE, identified in the months of April, May and June over the subcontinent, may also explain a significant portion of the general surface temperature variability, sometimes even during the maximum heat wave period. At this point, following previous modeling studies, it is noted that at around 25° latitude, heat waves associated with extreme geopotential anomalies may take effect only in a couple of days as compared to almost a week at higher latitudes (Jiménez-Esteve & Domeisen, 2022; Lau & Nath, 2014). Also the maximum in T_{max} is found to be co-eval with the maximum in the geopotential height anomaly (ΔGH) (Jiménez-Esteve & Domeisen, 2022). That is, any lag, of the extreme T_{max}, more than a couple of days from the development of statistically significant positive ΔGH may be indicative of other controlling processes. These studies also show that at 25° latitude, the mid tropospheric ΔGH associated with heat waves could be around 30 m, which can increase to up to 100 m at higher latitudes.

Figure 8 shows the May 2016 time series of several meteorological variables over Phalodi, Rajasthan, India. The variables q_z, pressure velocity at 550 hPa (ω_{550}) and CRF derived from ERA5, averaged over a 2°×2° region centered around Phalodi are used to understand the IWVE. Following studies of extra-tropical heat waves, the geopotential height anomalies from a climatological mean (1979 to 2020) at 800 hPa and 550 hPa (ΔGH_{800}, ΔGH_{550}) are used to represent the role of blocking highs in triggering heat stress. Figure S7 shows the same variables over other regions in the subcontinent during the same heat wave. These regions were chosen because they have either a high IWVE, ΔT_{max} or ΔGH_{550} signal. These figures are summarised in Table 1.

The IWVE correlations, either with q_{sfc} or with CWV are moderately high and statistically significant for all stations during May 2016. The correlation between T_{max} and GH_{550} is smaller and mostly insignificant at all stations. The highest T_{max} anomalies appear around 17^{th} to 19^{th} May, except in Dachepalli in eastern India. The onset of significant ΔT_{max} usually lags significant ΔGH_{550} by around 4-7 days at all stations except Dachepalli where the heat wave starts right after a period of heavy precipitation. Except for Phalodi, no station has a significant ΔGH_{550} on the day of the maxima in T_{max}. But, for Phalodi, although the period of maximum T_{max} is co-eval with a significant ΔGH_{550}, the maxima in ΔGH_{550} occurs 10 days earlier. Some stations like Lucknow and Maharashtra don't show a persistent multi-day positive ΔGH_{550} preceding or co-eval with the heat wave. In most cases, the period of significant positive ΔGH_{550} or ΔT_{max} are not associated with statistically significant downwelling. However, during the period of significant ΔT_{max} the CRF is, in general, low in magnitude as compared to the rest of the month or even maximum positive for Gujarat during this period. The rest of the month is marked by larger negative CRF in general. It is noteworthy that this period of low CRF does not coincide with the period of significant positive ΔGH_{550}.

The above preliminary analysis suggests that statistically significant geopotential anomalies are not co-eval with the period of highest heat stress at least over the Indian subcontinent during the severe heat wave of May 2016. In fact, these periods may be separated from each other by several days. At the same time, every station is found to be significantly impacted by the IWVE, especially during extremes in surface temperatures. This observation, although does not preclude the possible role of a blocking high in impacting the heat wave, does provide support for the role of the tropics-wide IWVE in causing regular heat stress throughout the pre-monsoon summer season, every year, contiguously throughout the tropics. This is observed in the Indian subcontinent, which regularly experiences pre-monsoon heat stress (Pai et al., 2013), which could have a dominant component from the continuously varying humidity resulting in extremes in temperature.

It should be noted that May 2016 was a severe pre-monsoon heat stress year for the Indian subcontinent, hence the atmosphere could be impacted by certain synoptic scale conditions, other than the IWVE, not considered in detail here. Moreover, this analysis does not consider positive feedback from dry soils which might add another layer of complexity to local T_{max} evolution (Miralles et al., 2014; Perkins, 2015). Hence, further investigation is needed to unravel the relative significance of these processes in causing heat stress at these latitudes.

4 Conclusion

This study shows the existence of regions at the borders of the inter-tropical convergence zone where the atmospheric dynamics seems to specifically support the occurrence of clouds with a negative radiative impact on daily maximum surface temperatures T_{max} in the current climate. Additionally, other clouds, known to have a positive radiative forcing, have tapering down occurrences in these same regions. Both, cloud areal coverage and surface cloud radiative forcing (CRF) have a positive correlation with lower tropospheric water vapor q_{sfc} in these regions. As a result, surface temperatures are strongly negatively correlated with water vapor. These regions, where water vapor has an apparent negative impact on surface warming, have been referred to as the regions of 'indirect water vapor effect' or IWVE.

Such a negative forcing from water vapor is not observed in any other extensive region outside this belt around the ITCZ which coincides with the horizontal branch of latitudinal overturning circulations, like the Hadley cell. The negative daily CRF may not be unique to the IWVE regions, however the strong positive correlation of q_{sfc} with CRF and negative correlation in turn with T_{max} is uniquely observed in the IWVE regions only. We suspect that in other regions, processes other than IWVE which impact T_{max} through q_{sfc}, may become important, but were not the focus of this study. The mechanism which lets water vapor to be dominantly, positively correlated with cloud occurrence of low and mid-level clouds in these regions, remains to be explored.

The IWVE regions occur on both sides of the ITCZ in all seasons and follow its annual north-to-south march. This means, periods where IWVE is active, both precede and succeed the monsoon in a tropical region. Although not addressed in detail in this study, this can have consequences for pre-monsoonal heat stress in regions like the Sahel in Africa, the Cerrado in South America and the Indian subcontinent where the IWVE is found active in this season which is already fraught with positive surface temperature feedback from receding soil moisture (Perkins, 2015; Pai et al., 2013; Miralles et al., 2014; Oueslati et al., 2017). The post monsoon occurrence of the IWVE may not have a substantial health impact because of the general lower surface temperatures due to wet soils and a receding sun after the monsoons. An in-depth analysis of the role of IWVE versus other mechanisms of pre-monsoon heat stress in these regions is required.

Lastly, The IWVE seems to have a connection with the horizontal branch of latitudinal overturning circulations in the tropics, in the way the latter affects cloud distribution. With evidence that tropical overturning circulations, like the Hadley cell, are set to change in a warmer climate (Lu et al., 2007), the IWVE and its associated impact on surface temperatures may evolve as well. An understanding of how this sensitive balance would be modified under global climate change could be important, especially because in the IWVE regions, this effect may be substantially associated with pre-monsoonal heat stress.

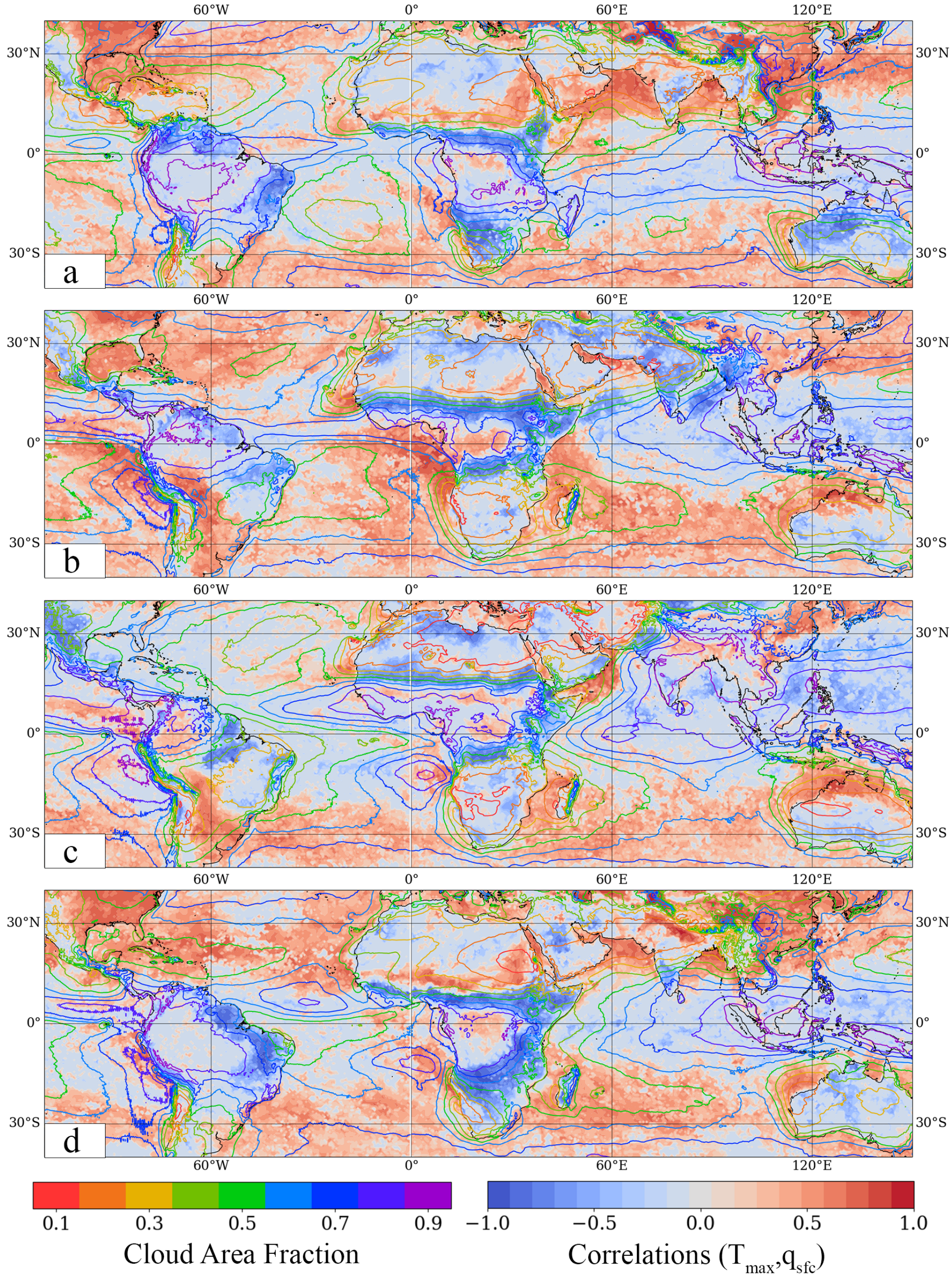

Figure 1. The tropical indirect water vapor negative radiative effect and its co-occurrence with transition regions in cloud fraction. Colored Shading - Mode of monthly daily scale correlations between daily T_{max} and q_{sfc} in (a) February, (b) May, (c) August, and (d) November. The mode was calculated from the population of all monthly correlations between 2001-2020. See methods for details. Colored line Contours – Average total cloud area fraction for the corresponding months between 2001 and 2020. All data from ERA5.

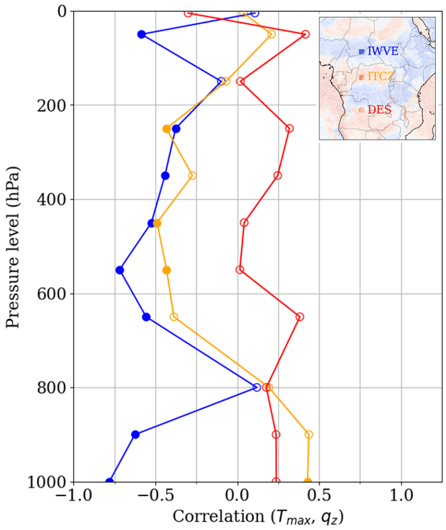

Figure 2. IWVE regions show negative correlations between T_{max} and upper tropospheric specific humidity. Correlation coefficients between daily T_{max} and daily average specific humidity at various altitudes, q_z, in May 2016 at selected IWVE, ITCZ and DES regions in Africa (inset). Data from ERA5. Correlations significant at the 95% confidence level are shown with filled circles.

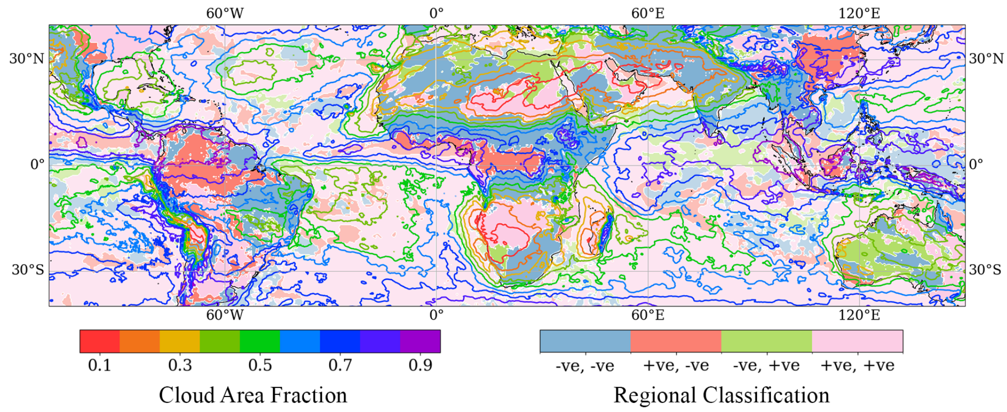

Figure 3. Dominant IWVE regions in the tropics. Classification of various regions into four types based on whether the sign of the grid scale correlations between daily T_{max} and q_{sfc} is the same as that between T_{max} and CWV. Area 1 - both negative, Area 2 - former positive, latter negative, Area 3 - negative, positive, Area 4 - both positive. Data obtained from ERA5 for May 2016 (compare this with Figure S1b). The map has an overlay of average cloud cover for May 2016. Ocean grid points have been de-saturated.

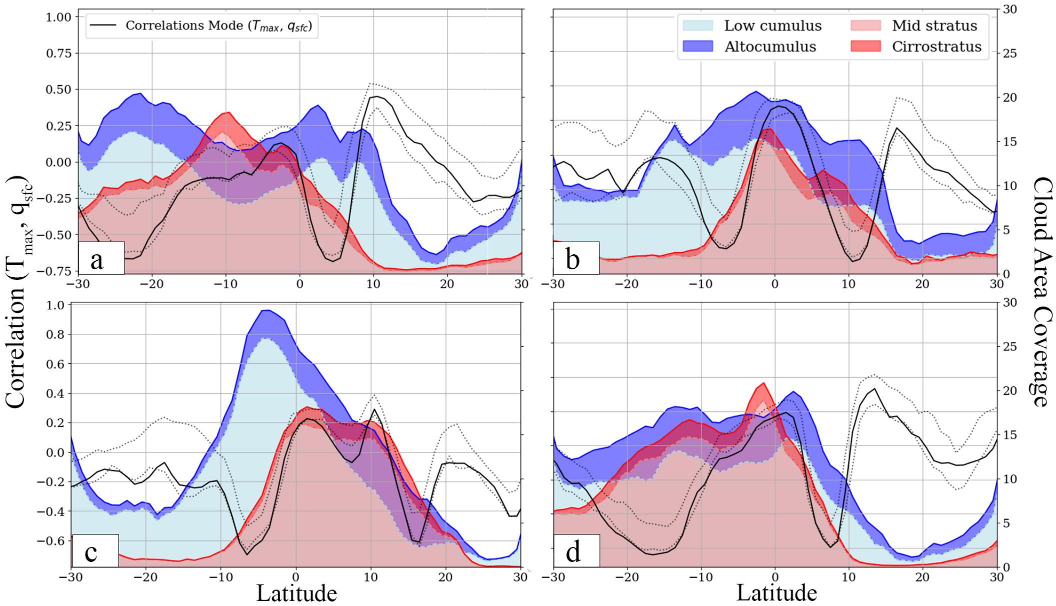

Figure 4. Dominant presence of mid level clouds in IWVE regions. Daytime cloud fraction over Africa, zonally averaged between 30°N, 17.5°E and 30°S, 30°E for (a) February, (b) May, (c) August, and (d) November, 2001 to 2020. Could types shown - Low cumulus including shallow cumulus (low, thin) and stratocumuls (low, medium thick); altocumulus (mid, thin); mid stratus including altostratus (mid, medium thickness) and nimbostratus (mid, thick); cirrostratus (high, medium thick). Data from CERES CldTypHist 1°×1° monthly average day time values. Cumulus and stratus clouds with the largest % area coverage have been shown, while other cloud species such as deep convection, nimbostratus and cirrus clouds have been omitted from this analysis due to their comparatively low area coverage (see Fig. S5). This is done assuming that clouds with small % area cover do not have dominant radiative effect at the surface.

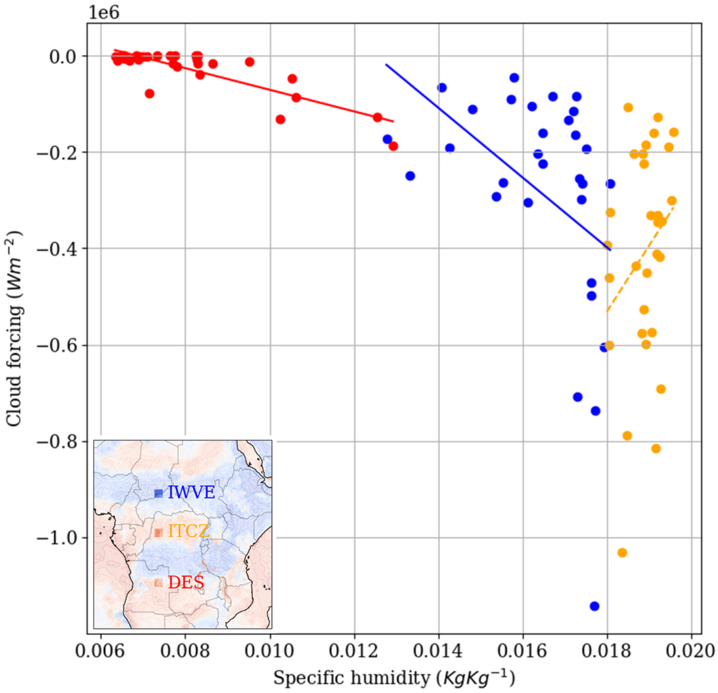

Figure 5. Surface cloud radiative forcing in IWVE regions is sensitive to near surface atmospheric humidity. Daytime averaged CRF versus q_{sfc} for a 1°×1° IWVE, ITCZ and a DES region in Africa (inset), for all days in May 2016. All data from ERA5.

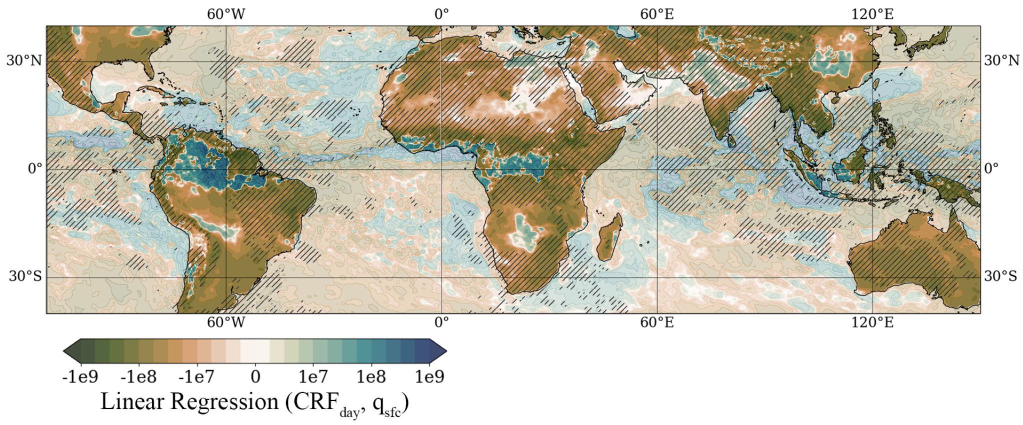

Figure 6. IWVE across tropics show a negative relation of surface humidity with cloud radiative forcing. Coefficients of linear regression of daytime CRF on daily averaged q_{sfc}. Regression performed with ERA5 grid scale, daily data for May 2016. Most values above -7e7 are significant at the 95% confidence level. Most positive regression coefficients are insignificant. Statistical significance is not shown to improve figure clarity. Hatching shows all regions with negative correlations between T_{max} and q_{sfc}. Data obtained from ERA5.

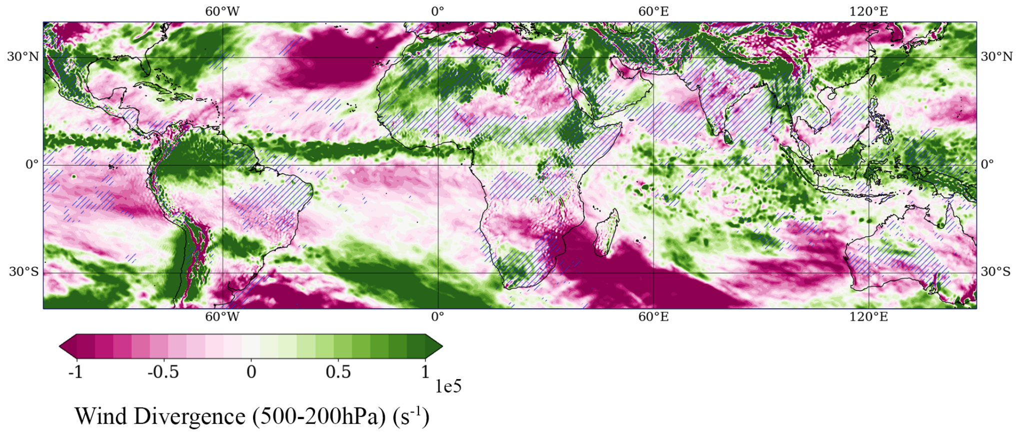

Figure 7. IWVE associated with the horizontal branch of continental scale overturning circulations. Shading shows the divergence of horizontal winds, column integrated between 500 hPa and 200 hPa averaged over May 2016. Hatching shows IWVE regions with T_{max}, q_{sfc} correlation coefficients between -1 and -0.5. Data obtained from ERA5.

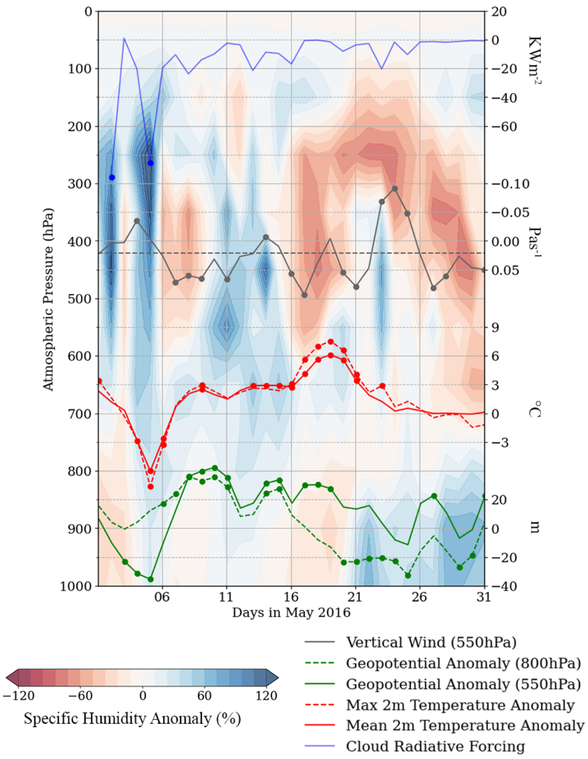

Figure 8. Severe tropical heat stress could be related to IWVE. Daily scale time series of T_{max}, T_{avg} (daily mean), GH_{800} and GH_{550} anomalies from the climatological mean corresponding to May 1979 to 2020. Figure also shows the percentage temporal anomalies in q_z from the monthly mean of May 2016, the daytime CRF and daily 550 hPa vertical wind ω_{550}. The dashed grey line represents the climatological average vertical wind in May. Significant anomalies are marked. Significant differences of CRF and ω_{550} from the monthly and climatological mean respectively are also marked. All variables derived from a 2°×2° area over Phalodi, north-western India in May 2016. Data obtained from ERA5.

Table 1. Importance of IWVE during the heat wave of May 2016 over the Indian subcontinent. Meteorological conditions during the May 2016 heat wave recorded in India. Statistics calculated using a month long daily scale time series of meteorological variables around centers of heat stress, with the same methodology as used in Figure 8. Meteorological conditions for two types of days are analyzed - day of the monthly maximum T_{max} and the day of the monthly maximum geopotential anomaly at 550 hPa, ΔGH_{550}. For the heat wave day values are reported for the daily maximum and averaged surface temperature anomalies from the climatological (1979 to 2020) monthly mean ΔT_{max} and ΔT_{avg}, daily scale IWVE correlations corr(T_{max},q_{sfc}) and corr(T_{max},CWV), daily scale area averaged vertical wind at 550 hPa ω_{550}, daytime averaged surface CRF, anomaly in the geopotential heights at the 800 hPa and 550 hPa levels during the heat wave period (ΔGH_{800}, ΔGH_{550}), and correlations corr(T_{max},GH_{800}) and corr(T_{max},GH_{550}). Some of these values are also reported for the day of maximum ΔGH_{550}. Statistics significant at the 95% confidence level are bold. All data from ERA5. All values are averaged over a 2°×2° area around the region under study.

	Phalodi	Datia	Lucknow	Dachepalli	Radhanpur	Patoda
latitude (°N)	27.13	25.67	26.87	16.5	23.75	18.75
longitude (°E)	72.36	78.45	80.94	79.75	71.75	75.5
avg($T_{avg,May}$)	34.96	34.05	33.78	33.2	33.7	32.38
Day of max(T_{max})	19	18	17	24	18	17
ΔT_{max} (°C)	**7.51**	**3.97**	**4.26**	**4.16**	**6.14**	**3.79**
ΔT_{avg} (°C)	**6.1**	**3.83**	**3.54**	**4.05**	**3.99**	**3.8**
corr(T_{max},q_{sfc})	**-0.4**	**-0.37**	**-0.47**	**-0.81**	**-0.37**	**-0.45**
corr(T_{max},CWV)	**-0.62**	**-0.41**	**-0.57**	**-0.67**	**-0.69**	-0.24
ω_{550} (Pa sec^{-1})	0.0	0.0	0.01	**0.03**	0.03	0.03
CRF (kW m^{-2})	-1.51	0	-19.1	-33.39	0.5	-18.97
ΔGH_{800} (m)	-13.16	-14.83	-11.04	3.86	-10.91	**-20.2**
ΔGH_{550} (m)	**27.6**	14.37	6.27	7.62	**19.74**	-2.96
corr(T_{max},GH_{800})	-0.2	**-0.39**	-0.17	0.33	0	-0.13
corr(T_{max},GH_{550})	**0.38**	0.17	0.32	**0.39**	**0.4**	0.31
Day of max(ΔGH_{550})	10	14	14	14	14	14
ΔT_{max} (°C)	2.27	**2.73**	**3.11**	1.01	**2.43**	**2.38**
ΔGH_{550} (m)	**42.33**	**35.53**	**35.22**	**29.9**	**32.01**	**34.9**
CRF (kW m^{-2})	-9.98	-31.9	-30.56	-22.33	0.28	-76.91

5 Open Research

[H] The meteorological data used for the heat stress analysis in the study is available freely on the Copernicus Climate Data Store via 10.24381/cds.143582cf, `https://cds.climate.copernicus.eu/#!/search?text=ERA5&type=dataset` (Hersbach et al., 2020, 2023). Supporting meteorological data from the AIRS L3 standard data products V7 is obtained from the data collections at NASA GES DISC via 10.5067/UO3Q64CTTS1U, `https://disc.gsfc.nasa.gov/datasets?page=1&source=AQUA%20AIRS&keywords=airs%20version%207` (AIRS, 2019). CERES cloud type and surface radiation flux data are obtained from the SYN1deg level 3 products from the NASA CERES data repository via (doi - 10.5067/TERRA+AQUA/CERES/CLDTYPHIS_L3.004, doi - 10.5067/Terra+Aqua/CERES/SYN1degDay_L3.004A respectively) `https://ceres.larc.nasa.gov/data/` (Doelling et al., 2013, 2016). All datasets used are available freely for public use.

All original Python (> 3.9) code will be archived if the manuscript is accepted and can be obtained from the repository or upon request from Karan at karan42mahajan@gmail.com. All data used from the above sources can also be separately obtained from Karan.

Acknowledgments
The authors acknowledge financial support from the National Institute of Science Education and Research, Bhubaneshwar, India and the Ministry of Education, Government of India, grant number MoE-STARS1/766.

References

Agarwal, V. (2016, 5). Indian heat wave breaks record for highest temperature. *The Wall Street Journal*. Retrieved from `https://www.wsj.com/articles/BL-IRTB-32135`

AIRS. (2019). *Airs project, aqua/airs l3 daily standard physical retrieval (airs-only) 1 degree x 1 degree v7.0 [dataset].* doi: 10.5067/UO3Q64CTTS1U

Alizadeh, M. R., Abatzoglou, J. T., Adamowski, J. F., Prestemon, J. P., Chittoori, B., Asanjan, A. A., & Sadegh, M. (2022, 2). Increasing heat-stress inequality in a warming climate. *Earth's Future*, *10*. doi: 10.1029/2021EF002488

Allan, R. P., Shine, K. P., Slingo, A., & Pamment, J. A. (1999, 7). The dependence of clear-sky outgoing long-wave radiation on surface temperature and relative humidity. *Quarterly Journal of the Royal Meteorological Society*, *125*, 2103-2126. doi: 10.1002/qj.49712555809

Araújo, I., Marimon, B. S., Scalon, M. C., Fauset, S., Marimon, B. H., Tiwari, R., ... Gloor, M. U. (2021, 3). Trees at the amazonia-cerrado transition are approaching high temperature thresholds. *Environmental Research Letters*, *16*. doi: 10.1088/1748-9326/abe3b9

Biemans, H., Siderius, C., Mishra, A., & Ahmad, B. (2016, 5). Crop-specific seasonal estimates of irrigation-water demand in south asia. *Hydrology and Earth System Sciences*, *20*, 1971-1982. doi: 10.5194/hess-20-1971-2016

Bouniol, D., Couvreux, F., Kamsu-Tamo, P. H., Leplay, M., Guichard, F., Favot, F., & O'connor, E. J. (2012, 3). Diurnal and seasonal cycles of cloud occurrences, types, and radiative impact over west africa. *Journal of Applied Meteorology and Climatology*, *51*, 534-553. doi: 10.1175/JAMC-D-11-051.1

Bourgeois, Q., Ekman, A. M., Igel, M. R., & Krejci, R. (2016, 8). Ubiquity and impact of thin mid-level clouds in the tropics. *Nature Communications*, *7*. doi: 10.1038/ncomms12432

Brutsaert, W. (1975, 10). On a derivable formula for long-wave radiation from clear skies. *Water Resources Research*, *11*, 742-744. doi: 10.1029/WR011i005p00742

Carmona, F., Rivas, R., & Caselles, V. (2014). Estimation of daytime downward longwave radiation under clear and cloudy skies conditions over a sub-humid region. *Theoretical and Applied Climatology*, *115*, 281-295. doi: 10.1007/s00704-013-0891-3

Chen, T., Rossow, W. B., & Zhang, Y. (2000, 1). Radiative effects of cloud-type variations. *Journal of Climate*, *13*, 264-286. doi: 10.1175/1520-0442(2000)013⟨0264:REOCTV⟩2.0.CO;2

Coffel, E. D., Horton, R. M., & Sherbinin, A. D. (2018, 1). Temperature and humidity based projections of a rapid rise in global heat stress exposure during the 21st century. *Environmental Research Letters*, *13*. doi: 10.1088/1748-9326/aaa00e

Coumou, D., Robinson, A., & Rahmstorf, S. (2013). Global increase in record-breaking monthly-mean temperatures. *Climatic Change*, *118*, 771-782. doi: 10.1007/s10584-012-0668-1

Derbyshire, S., Beau, I., Bechtold, P., Grandpeix, J.-Y., Piriou, J.-M., Redelsperger, J.-L., & Soares, P. (2004, 10). Sensitivity of moist convection to environmental humidity. *Quarterly Journal of the Royal Meteorological Society*, *130*, 3055-3079. doi: 10.1256/qj.03.130

de Rooy, W. C., Bechtold, P., Fröhlich, K., Hohenegger, C., Jonker, H., Mironov, D., ... Yano, J. I. (2013, 1). Entrainment and detrainment in cumulus convection: An overview. *Quarterly Journal of the Royal Meteorological Society*, *139*, 1-19. doi: 10.1002/qj.1959

Dessler, A. E., Schoeberl, M. R., Wang, T., Davis, S. M., & Rosenlof, K. H. (2013, 11). Stratospheric water vapor feedback. *Proceedings of the National Academy of Sciences of the United States of America*, *110*, 18087-18091. doi: 10.1073/pnas.1310344110

Doelling, D. R., Loeb, N. G., Keyes, D. F., Nordeen, M. L., Morstad, D., Nguyen, C., ... Sun, M. (2013, 6). Geostationary enhanced temporal interpolation for ceres flux products [dataset]. *Journal of Atmospheric and Oceanic Technology*, *30*, 1072-1090. doi: 10.1175/JTECH-D-12-00136.1

Doelling, D. R., Sun, M., Nguyen, L. T., Nordeen, M. L., Haney, C. O., Keyes, D. F., & Mlynczak, P. E. (2016, 3). Advances in geostationary-derived longwave fluxes for the ceres synoptic (syn1deg) product [dataset]. *Journal of Atmospheric and Oceanic Technology*, *33*, 503-521. doi: 10.1175/JTECH-D-15-0147.1

Douglas, E. M., Beltrán-Przekurat, A., Niyogi, D., Pielke, R. A., & Vörösmarty, C. J. (2009, 5). The impact of agricultural intensification and irrigation on land-atmosphere interactions and indian monsoon precipitation - a mesoscale modeling perspective. *Global and Planetary Change*, *67*, 117-128. doi: 10.1016/j.gloplacha.2008.12.007

Douglas, E. M., Niyogi, D., Frolking, S., Yeluripati, J. B., Pielke, R. A., Niyogi, N., ... Mohanty, U. C. (2006). Changes in moisture and energy fluxes due to agricultural land use and irrigation in the indian monsoon belt. *Geophysical Research Letters*, *33*. doi: 10.1029/2006GL026550

Dunne, J. P., Stouffer, R. J., & John, J. G. (2013, 6). Reductions in labour capacity from heat stress under climate warming. *Nature Climate Change*, *3*, 563-566. doi: 10.1038/nclimate1827

Findell, K. L., & Eltahir, E. A. B. (2003a). Atmospheric controls on soil moisture-boundary layer interactions. part i: Framework development. *Journal of Hydrometeorology*, *4*, 552-569. doi: 10.1175/1525-7541(2003)004⟨0552:acosml⟩2.0.co;2

Findell, K. L., & Eltahir, E. A. B. (2003b, 6). Atmospheric controls on soil moisture–boundary layer interactions. part ii: Feedbacks within the continental united states. *Journal of Hydrometeorology*, *4*, 570-583. doi: 10.1175/1525-7541(2003)004⟨0570:ACOSML⟩2.0.CO;2

Flerchinger, G. N., Xaio, W., Marks, D., Sauer, T. J., & Yu, Q. (2009, 3). Comparison of algorithms for incoming atmospheric long-wave radiation. *Water Resources Research*, *45*. doi: 10.1029/2008WR007394

Forster, P., Storelvmo, T., Armour, K., Collins, W., Dufresne, J.-L., Frame, D., ... Zhang, H. (2021, 7). The earth's energy budget, climate feedbacks and climate sensitivity. In (p. 923-1054). Cambridge University Press. Retrieved from `https://www.cambridge.org/core/product/identifier/9781009157896%23c7/type/book_part` doi: 10.1017/9781009157896.009

Gaffen, D. J., Elliott, W. P., & Robock, A. (1992, 9). Relationships between tropospheric water vapor and surface temperature as observed by radiosondes. *Geophysical Research Letters*, *19*, 1839-1842. doi: 10.1029/92GL02001

Hartmann, D. L., Ockert-Bell, M. E., & Michelsen, M. L. (1992, 11). The effect of cloud type on earth's energy balance: Global analysis. *Journal of Climate*, *5*, 1281-1304. doi: 10.1175/1520-0442(1992)005⟨1281:TEOCTO⟩2.0.CO;2

Hersbach, H., Bell, B., Berrisford, P., Biavati, G., Horányi, A., Sabater, J. M., ... Thépaut, J.-N. (2023). *Era5 hourly data on pressure levels from 1940 to present [dataset].* doi: https://doi.org/10.24381/cds.bd0915c6

Hersbach, H., Bell, B., Berrisford, P., Hirahara, S., Horányi, A., Muñoz-Sabater, J., ... Thépaut, J. (2020, 7). The era5 global reanalysis [dataset]. *Quarterly Journal of the Royal Meteorological Society*, *146*, 1999-2049. doi: 10.1002/qj.3803

Hoegh-Guldberg, O., Jacob, D., Taylor, M., Bindi, M., Brown, S., Camilloni, I., ... Zhou, G. (2018). *Impacts of 1.5 ºc global warming on natural and human systems global warming of 1.5°c. an ipcc special report on the impacts of global warming of 1.5°c above pre-industrial levels and related global greenhouse gas emission pathways, in the context of strengthening the global response to the threat of climate change, sustainable development, and efforts to eradicate poverty, ipcc.*

Holloway, C. E., Neelin, J. D., Holloway, C. E., & Neelin, J. D. (2009, 6). Moisture vertical structure, column water vapor, and tropical deep convection. *Journal of the Atmospheric Sciences*, *66*, 1665-1683. doi: 10.1175/2008JAS2806.1

Im, E. S., Pal, J. S., & Eltahir, E. A. (2017, 8). Deadly heat waves projected in the densely populated agricultural regions of south asia. *Science Advances*, *3*. doi: 10.1126/sciadv.1603322

IMD. (2002, 2). *Recommendation regarding the revised criteria for declaring heat wave/ cold wave, ddgm (wf).*

Iwasa, Y., Arakawa, T., & Sumi, A. (2012). Tropospheric mid-level detrainment flow obtained from high-resolution non-hydrostatic atmospheric model experiments. *Journal of the Meteorological Society of Japan. Ser. II*, *90*, 11-33. doi: 10.2151/jmsj.2012-102

Jiménez-Esteve, B., & Domeisen, D. I. (2022, 7). The role of atmospheric dynamics and large-scale topography in driving heatwaves. *Quarterly Journal of the Royal Meteorological Society*, *148*, 2344-2367. doi: 10.1002/qj.4306

Johnson, R. H., Ciesielski, P. E., & Hart, K. A. (1996, 7). Tropical inversions near the 0°c level. *Journal of the Atmospheric Sciences*, *53*, 1838-1855. doi: 10.1175/1520-0469(1996)053⟨1838:TINTL⟩2.0.CO;2

Johnson, R. H., Rickenbach, T. M., Rutledge, S. A., Ciesielski, P. E., & Schubert, W. H. (1999). *Trimodal characteristics of tropical convection.*

Lau, N.-C., & Nath, M. J. (2014, 5). Model simulation and projection of european heat waves in present-day and future climates. *Journal of Climate*, *27*, 3713-3730. doi: 10.1175/JCLI-D-13-00284.1

Lawston, P. M., Santanello, J. A., Hanson, B., & Arsensault, K. (2020). Impacts of irrigation on summertime temperatures in the pacific northwest. *Earth Interactions d*, *24*. doi: 10.1175/EI-D-19-0015.s1

Li, D., Yuan, J., & Kopp, R. E. (2020, 6). Escalating global exposure to compound heat-humidity extremes with warming. *Environmental Research Letters*, *15*.

doi: 10.1088/1748-9326/ab7d04

Li, M., Liao, Z., & Coimbra, C. F. (2018, 4). Spectral model for clear sky atmospheric longwave radiation. *Journal of Quantitative Spectroscopy and Radiative Transfer*, *209*, 196-211. doi: 10.1016/j.jqsrt.2018.01.029

Li, X. X. (2020, 6). Heat wave trends in southeast asia during 1979–2018: The impact of humidity. *Science of the Total Environment*, *721*. doi: 10.1016/j.scitotenv.2020.137664

Lobell, D. B., & Bonfils, C. (2008, 5). The effect of irrigation on regional temperatures: A spatial and temporal analysis of trends in california, 1934-2002. *Journal of Climate*, *21*, 2063-2071. doi: 10.1175/2007JCLI1755.1

Lobell, D. B., Bonfils, C., & Faurès, J. M. (2008). The role of irrigation expansion in past and future temperature trends. *Earth Interactions*, *12*. doi: 10.1175/2007EI241.1

Lu, J., Vecchi, G. A., & Reichler, T. (2007, 3). Expansion of the hadley cell under global warming. *Geophysical Research Letters*, *34*, L06805. doi: 10.1029/2006GL028443

Mahlstein, I., Knutti, R., Solomon, S., & Portmann, R. W. (2011). Early onset of significant local warming in low latitude countries. *Environmental Research Letters*, *6*. doi: 10.1088/1748-9326/6/3/034009

Mazdiyasni, O., AghaKouchak, A., Davis, S. J., Madadgar, S., Mehran, A., Ragno, E., ... Niknejad, M. (2017, 6). Increasing probability of mortality during indian heat waves. *Science Advances*, *3*. doi: 10.1126/sciadv.1700066

Miralles, D. G., Teuling, A. J., Heerwaarden, C. C. V., & Arellano, J. V. G. D. (2014). Mega-heatwave temperatures due to combined soil desiccation and atmospheric heat accumulation. *Nature Geoscience*, *7*, 345-349. doi: 10.1038/ngeo2141

Oldenborgh, G. J. V., Philip, S., Kew, S., Weele, M. V., Uhe, P., Otto, F., ... Achutarao, K. (2018, 1). Extreme heat in india and anthropogenic climate change. *Natural Hazards and Earth System Sciences*, *18*, 365-381. doi: 10.5194/nhess-18-365-2018

Oueslati, B., Pohl, B., Moron, V., Rome, S., & Janicot, S. (2017, 5). Characterization of heat waves in the sahel and associated physical mechanisms. *Journal of Climate*, *30*, 3095-3115. doi: 10.1175/JCLI-D-16-0432.1

Pai, D. S., Nair, A., & Ramanathan, A. N. (2013). *Long term climatology and trends of heat waves over india during the recent 50 years (1961-2010)* (Vol. 64).

Parker, D. J., Willetts, P., Birch, C., Turner, A. G., Marsham, J. H., Taylor, C. M., ... Martin, G. M. (2016, 7). The interaction of moist convection and mid-level dry air in the advance of the onset of the indian monsoon. *Quarterly Journal of the Royal Meteorological Society*, *142*, 2256-2272. doi: 10.1002/qj.2815

Perkins, S. E. (2015, 10). *A review on the scientific understanding of heatwaves-their measurement, driving mechanisms, and changes at the global scale* (Vol. 164-165). Elsevier Ltd. doi: 10.1016/j.atmosres.2015.05.014

Puma, M. J., & Cook, B. I. (2010). Effects of irrigation on global climate during the 20th century. *Journal of Geophysical Research Atmospheres*, *115*. doi: 10.1029/2010JD014122

Ramanathan, V., Cess, R. D., Harrison, E. F., Minnis, P., Barkstrom, B. R., Ahmad, E., & Hartmann, D. (1989, 1). Cloud-radiative forcing and climate: Results from the earth radiation budget experiment. *Science*, *243*, 57-63. doi: 10.1126/science.243.4887.57

Ratnam, J. V., Behera, S. K., Ratna, S. B., Rajeevan, M., & Yamagata, T. (2016, 4). Anatomy of indian heatwaves. *Scientific Reports*, *6*. doi: 10.1038/srep24395

Reich, P. B., Sendall, K. M., Rice, K., Rich, R. L., Stefanski, A., Hobbie, S. E., & Montgomery, R. A. (2015, 1). Geographic range predicts photosynthetic and growth response to warming in co-occurring tree species. *Nature Climate*

Change, *5*, 148-152. doi: 10.1038/nclimate2497
Riihimaki, L. D., Mcfarlane, S. A., & Comstock, J. M. (2012, 10). Climatology and formation of tropical midlevel clouds at the darwin arm site. *Journal of Climate*, *25*, 6835-6850. doi: 10.1175/JCLI-D-11-00599.1
Rohini, P., Rajeevan, M., & Srivastava, A. K. (2016, 5). On the variability and increasing trends of heat waves over india. *Scientific Reports*, *6*. doi: 10.1038/srep26153
Ross, R. J., Elliott, W. P., Seidel, D. J., & Grou, P. A.-I. M. (2002, 2). Lower-tropospheric humidity–temperature relationships in radiosonde observations and atmospheric general circulation models. *Journal of Hydrometeorology*, *3*, 26-38. doi: 10.1175/1525-7541(2002)003⟨0026:LTHTRI⟩2.0.CO;2
Schiro, K. A., Neelin, J. D., Adams, D. K., & Lintner, B. R. (2016). Deep convection and column water vapor over tropical land versus tropical ocean: A comparison between the amazon and the tropical western pacific. *Journal of the Atmospheric Sciences*, *73*, 4043-4063. doi: 10.1175/jas-d-16-0119.1
Shakespeare, C. J., & Roderick, M. L. (2021, 10). The clear-sky downwelling longwave radiation at the surface in current and future climates. *Quarterly Journal of the Royal Meteorological Society*, *147*, 4251-4268. doi: 10.1002/qj.4176
Soden, B. J., Jackson, D. L., Ramaswamy, V., Schwarzkopf, M. D., & Huang, X. (2005, 11). The radiative signature of upper tropospheric moistening. *Science*, *310*, 841-844. doi: 10.1126/science.1115602
Soden, B. J., Wetherald, R. T., Stenchikov, G. L., & Robock, A. (2002, 4). Global cooling after the eruption of mount pinatubo: A test of climate feedback by water vapor. *Science*, *296*, 727-730. doi: 10.1126/science.296.5568.727
Stein, T. H., Parker, D. J., Delanoë, J., Dixon, N. S., Hogan, R. J., Knippertz, P., ... Marsham, J. H. (2011). The vertical cloud structure of the west african monsoon: A 4 year climatology using cloudsat and calipso. *Journal of Geophysical Research Atmospheres*, *116*. doi: 10.1029/2011JD016029
Tharoor, I. (2016, 4). Brutal heat wave in india puts 330 million people at risk. *Washington Post*.
Tiwari, R., Gloor, E., da Cruz, W. J. A., Marimon, B. S., Marimon-Junior, B. H., Reis, S. M., ... Galbraith, D. (2021, 7). Photosynthetic quantum efficiency in south-eastern amazonian trees may be already affected by climate change. *Plant Cell and Environment*, *44*, 2428-2439. doi: 10.1111/pce.13770
Wehner, M., Stone, D., Krishnan, H., AchutaRao, K., & Castillo, F. (2016). The deadly combination of heat and humidity in india and pakistan in summer 2015. *Bulletin of the American Meteorological Society*, *97*, S81–S86. doi: 10.1175/Bams-D-16-0145.1
Wu, H. (2016, 5). Mercury rising: India records its highest temperature ever. *Cable News Network*.

An indirect, negative radiative effect of water vapor in the tropics and its implications for regional surface heat stress

J. Khanna[1,2], Karan[1,2]

[1]School of Earth and Planetary Sciences, National Institute of Science Education and Research, Jatni, 752050, India
[2]Homi Bhabha National Institute, Training School Complex, Anushaktinagar, Mumbai, 400094, India

Key Points:

- An indirect, water vapor related surface cooling is observed at the daily scale, pan-tropics, bordering the ITCZ, throughout the year
- Lower tropospheric humidity is negatively related with local cloud radiative forcing in these regions dominated by mid level clouds
- Regions occur along the horizontal branch of Hadley cell, move with the seasonal cycle, possibly consequential for pre-monsoon heat stress

Corresponding author: Jaya Khanna, `jkhanna@niser.ac.in`

Abstract

We report an indirect, negative, cloud-mediated, surface radiative effect (RE) of water vapor (IWVE) in certain regions in the tropics, which may be consequential for day-to-day regional heat stress. Using reanalysis and satellite data we show that this effect is marked by a surprisingly dominant positive relationship of cloud RE with near surface and column humidity. These clouds are predominantly low level and altocumuli, previously reported to have a negative surface RE, possibly lending the net negative RE to water vapor. Also reported earlier, these clouds form in the mid-troposphere, as detrainment offshoots of deep convective towers and can be advected away to large distances, hence requiring no local convective triggering in the IWVE regions. Evidently, the IWVE are co-located with the horizontal branch of the Hadley cell, with the lowest vertical forcing in the tropics. Moreover, these are also the transition regions between the highly cloudy and the driest parts of the tropics, with a waning down occurrence of cirrus, deep convective and altostratus clouds, linked with positive RE, corroborating the hypothesis. IWVE regions also show a large temporal variability in humidity possibly providing opportunity for a large variability in cloud fractional coverage, however the mechanism controlling this covariability is not understood. The IWVE is tightly tied with the seasonal cycle of the ITCZ and hence is likely a dominant source of pre-monsoon surface temperature variability and heat stress in the current climate. The evolution of the IWVE under future climate warming needs further investigation.

Plain Language Summary

The greenhouse radiative effect of water vapor on surface temperatures is widely known. However, can water vapor cause an ‘apparent’ radiative cooling effect under certain conditions? Here, we show that in certain extensive tropical regions, bordering the ITCZ, the lower tropospheric water vapor has a substantial relation with cloud occurrence, which subsequently renders an indirect surface cooling effect in high humidity conditions. These clouds are majorly shallow and mid level cumuli, which are known to have a negative surface radiative forcing. What causes the positive relation between lower tropospheric humidity and these clouds, is not understood. However, that these regions border the ITCZ and hence are co-located with the horizontal branch of the Hadley cell, suggests low amounts of convective triggering and hence high level clouds. The potentially reduced warming from the high level clouds may give the lower level clouds an upper hand in the net radiative impact. Lastly, these regions precede the ITCZ in time as they move north-south with it. This may be consequential for pre-monsoonal heat stress in tropical regions.

1 Introduction

Water vapor is frequently dubbed as the most important greenhouse gas which plays a dominant role in climate change through the water vapor feedback (Soden et al., 2002, 2005; Forster et al., 2021; Dessler et al., 2013). This control is delivered through the dominant impact of the increase in the upper tropospheric humidity on trapping the outgoing longwave radiation (OLR) and recycling it within the climate system (Soden et al., 2005; Allan et al., 1999; Dessler et al., 2013). This trapping of energy warms up all components of the climate system - the atmosphere, land and oceans. However, on hourly to daily time scales, it is the near surface humidity (or column integrated water vapor, as they are strongly correlated) which dominates the greenhouse effect of water vapor as manifested at the land surface (Shakespeare & Roderick, 2021; Flerchinger et al., 2009; M. Li et al., 2018; Brutsaert, 1975; Carmona et al., 2014). Idealized modeling studies of clear sky surface downwelling longwave radiation (DLR) are able to explain about 97% of the temporal variability in DLR with near surface humidity (q_{sfc}) and surface temperatures (T_{sfc}) (Shakespeare & Roderick, 2021). High positive correlations have been reported between in-situ observed q_{sfc} and DLR (or T_{sfc}), at daily to monthly time scales, in all sky conditions (Gaffen et al., 1992; Ross et al., 2002; M. Li et al., 2018). However, exceptions to this behavior (Ross et al., 2002), relatively understudied, highlight the role of the several other complex climatic processes that water vapor involves itself in - surface evapotranspiration, cloud formation, convective amplification etc - in impacting T_{sfc}. The resulting processes may modulate the initial water vapor greenhouse effect at regional scales. We set out to investigate this regionality in the 'effective' water vapor greenhouse effect, particularly in the tropics, and investigate the role of clouds in causing the exceptional behavior.

This study is motivated by the need to understand the regionality in the q_{sfc}-T_{sfc} relationship, to better analyse the recent increase in global heat stress (Alizadeh et al., 2022; Pai et al., 2013; Mazdiyasni et al., 2017; X. X. Li, 2020; D. Li et al., 2020), which is predicted to increase to deadly levels in tropical latitudes under climate change, especially in transition regions like the Sahel, the Cerrado and southern Asia (Coffel et al., 2018; Mahlstein et al., 2011; Coumou et al., 2013; Hoegh-Guldberg et al., 2018) affecting low income communities and ecosystems of these regions (Alizadeh et al., 2022; Dunne et al., 2013). Over the Amazon-Cerrado boundary in Brazil, trees are reported to be close to their threshold temperature for photosynthesis, already impacting these ecosystems during high heat stress conditions (Araújo et al., 2021; Tiwari et al., 2021; Reich et al., 2015). Over the densely populated southern Asia, pre-monsoon heat stress has emerged as a major challenge under climate change (Rohini et al., 2016; Pai et al., 2013). These regions are additionally impacted by the combined effects of high temperature and humidity on perceived heat, corroborating the challenge even further (Oldenborgh et al., 2018; Wehner et al., 2016; Im et al., 2017). This surmounting evidence raises the need to understand the impact of near surface humidity on surface temperatures and the covariability between them.

Over and above the impact of near surface humidity on DLR, discussed above, q_{sfc} can impact T_{sfc} through other processes that control surface warming. For example, it is suggested that evaporative cooling from intense irrigation, which will probably result in a negative correlation between the two variables, can cause a muted local warming of the surface (Oldenborgh et al., 2018; Lobell & Bonfils, 2008; Lobell et al., 2008; Puma & Cook, 2010; Douglas et al., 2009; Lawston et al., 2020). However, this process is applicable to regional scales only, where a substantial amount of irrigation is practiced, which is expected only in a small part of the tropics. Additionally, this process takes effect only in the dry season of the region when precipitation is low (Biemans et al., 2016; Douglas et al., 2006). Hence, a large spatial and temporal scale impact is not expected from this mode of surface cooling, especially not in the pre-monsoon season, when agriculture is anyways low due to the low supply of riverine or ground waters for irrigation, and high heat stress conditions (Biemans et al., 2016).

Lower tropospheric humidity is also crucial in cloud formation and hence can potentially influence CRF at regional scales, a relationship which we set out to investigate in this study. As an example of the former relationship, q_{sfc} plays the lead role in convective triggering, supporting conditions conducive to moist convection by reducing convective inhibition - a higher near surface moisture has been shown to have a positive impact on moist convection and cumulus clouds (Findell & Eltahir, 2003a, 2003b). Free tropospheric humidity above the boundary layer is also shown to support moist convection by reducing the detrainment drying of convective plumes (Derbyshire et al., 2004; de Rooy et al., 2013; Holloway et al., 2009; Schiro et al., 2016). However, such positive impact of q_{sfc} on cloud formation could be marred by other complex processes like prevailing atmospheric stability and horizontal advection, which may interfere with the relation between these variables in regions outside the tropical deep convection belt. In other words, humidity-cloud relationships may or may not be the same as the above for non-convective clouds. In this study, we show the existence of extended regions in the tropics where q_{sfc} and CWV are dominantly, positively correlated with shallow to mid tropospheric clouds which are reported, by previous studies, to have a negative surface radiative forcing (Bourgeois et al., 2016; Bouniol et al., 2012; Riihimaki et al., 2012; Stein et al., 2011; Parker et al., 2016). These regions thereby show an 'effective', net negative radiative impact of q_{sfc} (CWV) on T_{sfc} on a daily scale, specifically in the pre-monsoon season when heat stress is at its highest at these latitudes.

Hence, this study focuses on understanding the impact of q_{sfc}, through its relation with local cloud cover, on daily scale surface heat stress in tropical regions during the peak, pre-monsoon, summer season. The general correlations between the humidity and surface temperature variables are presented first, subsequently relating the observation to the local cloud cover and variability. Next, the relationship of these correlations with the larger scale atmospheric dynamics is presented. Lastly, a short analysis is presented to propose a possible role of the near surface humidity in causing observed heat stress through the processes identified.

2 Methods

This study focuses on processes that impact the daily scale variability of regional surface temperatures (T_{sfc}). As such, most analysis uses daily scale data for a selected month. This choice of time scales reflects our interest in the 'instantaneous' response of T_{sfc} to the radiative forcing by the variability in water vapor and clouds. Since the latter process takes of the order of a few hours to manifest, the day-to-day co-variability in the variables is analyzed, if not the co-variability at sub-daily time scales. The atmospheric water vapor variability at longer time scales might itself be caused by inter-seasonal and inter-annual climate variability and climate change, but that is not the focus of this study. However, our analysis with inter-annual, monthly averaged variables results in similar inferences as the analysis with daily scale variables, providing support for the generalizability of the processes identified. Results are majorly reported from the pre-monsoon summer season of the northern hemisphere, but the inferences remain unchanged for other seasons. The month of May 2016 is chosen for some specific analysis that is limited by the size of the data set involved. 2016 was a post El Niño year transitioning to a mild La Niña, infested by high heat stress in the Indian subcontinent (Oldenborgh et al., 2018).

Surface heat stress is quantified with daily scale maximum surface temperatures (T_{max}) from reanalysis and satellite datasets. T_{max} appears frequently and takes an important role in the formal estimation of heat stress (IMD, 2002; Perkins, 2015). However, in this study, heat stress is used to refer to periods of statistically significant departures of T_{max} from the climatological or monthly mean and should not be confused with the various heat wave indices used by meteorological departments to declare periods of heat stress. Most inferences reported here with T_{max} remain unchanged for an analysis with daily averaged surface temperatures (T_{avg}) and daily maximum 2 m air temperature ($T_{2m,max}$).

The daily averaged near surface specific humidity (q_{sfc}), specific humidity at various altitudinal levels (q_z) and total column water vapor (CWV) are used to capture the radiative effect of atmospheric water vapor on surface temperatures. Previous studies have utilized these variables to show that at daily to monthly timescales, in most global land areas these variables are non-linearly but positively correlated with the surface downwelling longwave radiation (DLR) or surface temperatures (Gaffen et al., 1992; Ross et al., 2002). Although the clear sky regression coefficients between q_{sfc} and DLR are space dependent (Allan et al., 1999), there is no previous evidence of them being negative. Hence, q_{sfc} is used to represent the greenhouse impact of atmospheric water vapor on surface temperatures (Shakespeare & Roderick, 2021).

ERA5 is the major source of daily and monthly average meteorological fields for the years 2001 to 2020 at a horizontal resolution of 0.25°×0.25° (Hersbach et al., 2020, 2023). Surface skin temperature and 1000 hPa specific humidity from the global analysis are used to represent T_{max} and q_{sfc} respectively. Supporting analysis is performed with Level 3 standard retrievals, version 7 from AIRS (AIRS, 2019) for the period 2001 to 2020 at a spatial resolution of 1°×1°. The daily daytime surface skin temperature from the ascending branch and daily near surface specific humidity averaged between the ascending (equator passing time - 1:30 pm LT) and descending (equator passing time - 1:30 am LT) branches are used to represent T_{max} and q_{sfc} respectively.

Cloud cover information is obtained from ERA5 at the same spatial resolution as that for T_{max} and q_{sfc}. Cloud fields are also obtained from CERES monthly average daytime cloud product, CldTypHist, for the period 2001 to 2020 at a spatial resolution of 1°×1° (Doelling et al., 2013, 2016). CERES CldTypHist characterizes clouds based on three altitude and three optical depth bins. The lowest level (1000 hPa to 680 hPa) has Cumulus, Stratocumulus and Stratus with optical depths 0.0-3.6, 3.6-23 and 23-380 respectively. The middle level (680 hPa to 440 hPa) has Altocumulus, Altostratus and Nimbostratus with optical depths 0.0-3.6, 3.6-23 and 23-380 respectively. The highest level (440 hPa to 10 hPa) have Cirrus, Cirrostratus and Deep Convective clouds with optical depths 0.0-3.6, 3.6-23 and 23-380 respectively. AIRS daily total cloud cover data is also used for the same analysis.

Surface cloud radiative forcing (CRF) is majorly estimated with hourly scale, daytime (6:00 am to 6:00 pm LT) surface radiative fluxes from ERA5. CERES SYN1deg level 3 product is also used to derive the daily scale CRF for May 2016 at a spatial resolution of 1°×1° (Doelling et al., 2013, 2016). The CRF is estimated as a difference between the all-sky and clear-sky net radiation at the surface (Ramanathan et al., 1989).

Most analysis in this work is performed using statistics like linear correlation coefficients, linear regressions coefficients and anomalies from spatio-temporal averages for daily scale data analyzed over a month. Statistical significance is obtained with a two-tailed t-test for correlation coefficients, linear regressions and differences at the 95% confidence level in all cases.

Some of the analysis is performed over the African subcontinent because the contiguous nature of this region across the equator into the two hemispheres provides the opportunity to investigate the processes studied along a meridian, without disruption from land-ocean boundaries and high topography. The generality of these processes, if applicable, over other continents is indicated by providing relevant details in the text.

Figures 1 and S1 show the multiyear mode of monthly correlations of daily scale T_{max} (or $T_{2m,max}$, T_{avg}) and q_{sfc} (or CWV). Multiyear mode is calculated using grid-scale monthly correlations for 20 years, from four neighboring grid points, regardless of the statistical significance of the correlations in individual years. However, the correlations of interest (IWVE correlations defined in 'Results and Discussion') are robustly significant across all years. Fig. S1b is shown as an example and will be discussed in detail in the next section.

3 Results and Discussion

The objective of this study is to identify regions where water vapor impacts surface heat stress through processes over and above its greenhouse warming impact. In other words, we endeavor to investigate regions where the direct greenhouse effect of water vapor may be masked by the radiative impacts of the other climatically important processes mediated by water vapor, like cloud formation. To identify such regions, a basic correlation analysis between daily scale surface temperature and indicators of atmospheric humidity is performed.

3.1 A negative correlation between near surface atmospheric water vapor and maximum daily surface temperatures

At the daily scale, T_{max} of a majority of regions around the globe are strongly positively correlated with q_{sfc} (Fig. 1), and CWV (Fig. S1 a) in ERA5 and also in AIRS (Fig. S2 a). The values of these correlation coefficients for May 2016, are displayed in Fig. S1 b to show that the spatial patterns of the multiyear mode of these correlations (Figs. 1, S1) compare well with the values for individual years. These widespread positive correlations could be attributed to the greenhouse effect of water vapor. The maximum positive correlations larger than ≈0.7 are obtained at high latitudes and moderate values over the tropical oceans, a feature of the surface temperature-humidity relationship reported before (Ross et al., 2002). The inhibition of these positive correlations along the inter-tropical convergence zone (ITCZ) over land could be attributable to the dominant presence of high level clouds in these regions, which may have a complex net CRF. The analysis of these regions is out of the scope of this study.

The same figures, however, also show several tropical and sub-tropical land regions with high, statistically significant, negative correlations between daily T_{max} and q_{sfc} which occur across seasons and the two data sets used. Such signal has previously been observed over western USA using radiosonde data (Ross et al., 2002). In our study the negative correlation coefficients range between -0.36 to -0.97 for data averaged for May between 2001 and 2020 (Fig. 1). The largest negative correlations are found predominantly over tropical Africa and tropical South America throughout the year and over the Indian subcontinent, southeast Asia and northern Australia in some seasons. Similar patterns appear also with T_{avg} and $T_{2m,max}$ (Figs. S1 c and S1 d) and with inter-annual correlations using monthly averaged data (Fig. S2 b), indicating the generalizability of this relationship. This apparent water vapor related cooling is observed over land areas on the flank regions of the ITCZ and follows its seasonal cycle (Fig. 1). Hence, for example over the Indian subcontinent, it comes into prominence in the dry, pre-monsoon summer season (Fig. S3). It should be noted however that these negative correlations might maximize in a region's peak monsoon period. This is probably due to an atmospheric moistening and a sharp evaporative surface cooling due to heavy precipitation - for example in June over India when the monsoons arrive over land (Fig. S3). However, the cause of the water vapor related cooling in the pre-monsoon dry period is not obvious.

This negative correlation of near surface water vapor with surface temperatures, suggesting an apparent negative radiative forcing from water vapor is termed here as the 'Indirect Water Vapor Effect' or IWVE. This apparent indirect forcing of water vapor is investigated next. In the following, IWVE correlations will mean a correlation between daily q_{sfc} and T_{max}, unless otherwise specified. Furthermore, the positive IWVE correlation regions over the deep convective regions near the equator are termed as the ITCZ and the positive IWVE correlation regions polewards of the IWVE regions are termed as the desert or DES regions.

Figure 2 shows the correlations between specific humidity at an altitude (q_z) and daily T_{max} over three regions of the African subcontinent - an IWVE, an ITCZ and a DES region in May 2016. These regions are carefully chosen to lie at the same longitude (19°E) and away from topography. Over the IWVE region, the correlation between T_{max} and q_z is always significantly negative throughout the troposphere. Similarly, over the DES region the above correlation is significantly positive throughout. However, over the ITCZ region the correlation is positive close to the surface but changes to negative in the upper half of the troposphere. The altitudinal dependence of the correlations over the ITCZ suggests a complex interplay of multiple processes, possibly involving clouds and water vapor, impacting surface temperatures, which is out of the scope of this study. Only the IWVE regions, where q_{sfc} dominates the overall correlation between CWV and T_{max}, are studied here. This is a reasonable choice because most IWVE regions defined based on Figures 1 and S1 also show a consistent negative correlation with CWV (Fig. 3).

3.2 IWVE regions occur between the cloudiest and clearest parts of the tropics

Figures 1, S1 and S2 also show an overlay of total cloud cover averaged over the indicated time periods from ERA5. The IWVE co-occurs with regions of transition cloud cover, tropics-wide, i.e. between regions of maximum and minimum cloud cover where its gradient is substantial. For example, during May over central Africa (Fig. 1 b), the average cloud cover over the IWVE regions is around 0.51 (standard deviation 0.17), as compared to around 0.71 (0.18) over the ITCZ and 0.24 (0.18) over the DES regions. Hence, the total cloud cover in the IWVE regions is intermediate between regions of predominant convection (ITCZ) and regions of predominant downwelling (over subtropical deserts like the Sahara, Kalahari, the Arabian desert etc). Additionally, the fact that the IWVE regions tightly border the equatorial regions of deep convection everywhere, and follow the north-south march of the ITCZ, suggests that the IWVE correlations could be mediated by the radiative effects of some specific clouds that are dominant at the borders of the ITCZ.

Next, a possible pathway, mediated by clouds, is analyzed, which may lead to the apparent negative radiative forcing from water vapor in the IWVE regions. These regions receive much lower precipitation than the ITCZ (Fig. S4) which suggests that the IWVE regions may harbor clouds, or a cloud distribution, that is distinctly different from those in the ITCZ, resulting in a distinctly different CRF. Clouds show a spectrum of surface and top of atmosphere CRF depending upon their cloud top height and optical depth (Chen et al., 2000; Hartmann et al., 1992). A radiative transfer calculation is often necessary to obtain the net radiative effect of a certain vertical distribution of clouds. However, in this study we have taken evidential support from previous research to tie the observed cloud distribution over the IWVE regions with the negative, apparently cloud-mediated radiative impact of q_{sfc}, both of which are discussed below. A comprehensive numerical analysis of these relationships is left for a follow up study.

3.3 IWVE regions are dominated by 'cooling' mid tropospheric clouds

Figure 4 shows the distribution of the daytime low, mid and high level clouds zonally averaged over a region in Africa (30°N, 17.5°E and 30°S, 30°E), obtained from the CERES CldTypHist product for May 2001 to 2020. The corresponding May average cloud maps for Africa are provided in Figure S5. There is a clear distinction in the distribution of different types of clouds between the ITCZ, IWVE and DES regions. The IWVE regions are marked by a dominant presence of low and mid level, optically thin to moderately thick clouds, like shallow cumuli, altocumuli and stratocumuli. While the ITCZ, apart from the low and mid level clouds, also have a higher percentage of optically thin to thick, mid and high clouds, relative to the IWVE regions. This feature is present in all seasons except when the IWVE correlations are large during the monsoon, apparently due to the presence of strong evaporative surface cooling (August in Northern Hemisphere in Figure 4c), in which case the low and altocumulus clouds become infrequent over the IWVE regions. Specifically, the non-monsoonal, IWVE regions show a dominant presence of mid level, low thickness altocumulus clouds, which follow the poleward boundaries of the IWVE regions and are present abundantly and uniformly between these latitudes (Figure S5 d).

The effective radiative impact of this disparate cloud distribution on surface temperatures over the IWVE, ITCZ and DES regions is expected to be different. Noticeably, low level shallow cumulus and mid level altocumulus and altostratus have been previously shown to have a negative radiative forcing on surface temperatures (Chen et al., 2000; Hartmann et al., 1992). Additionally, the predominant occurrence of thin (optical depth around 1.03) mid level clouds (3 to 8 km) with a possibly negative radiative forcing over land has been previously reported in the pre-monsoon months over western Africa in the Nigerian region (Bouniol et al., 2012; Bourgeois et al., 2016; Stein et al., 2011), in Darwin (Riihimaki et al., 2012) and in the pre-monsoon Indian subcontinent (Parker et al., 2016). These mid level, thin, altocumulus clouds with a negative radiative forcing in the tropical regions (Bourgeois et al., 2016), are associated with mid level detrainment from deep convective clouds near the zero degree isotherm (Johnson et al., 1996, 1999; Iwasa et al., 2012). It is suggested that the latent heat of condensation to ice causes the deep convective tower to lose buoyancy and form these clouds, which can get horizontally advected to far away regions. As such, the occurrence and radiative impact of such mid level clouds is likely to be important in the flank regions of the equatorial deep convective belt, which is where the IWVE regions occur.

Hence, the dominant shallow- and alto- cumulus clouds in the IWVE regions could be responsible for the observed surface cooling. However, the question - how is q_{sfc} in the IWVE regions linked to surface cooling caused through these clouds? - is still open. This is an important question, because the expected positive, greenhouse radiative forcing of water vapor seems to be negated by a mechanism that supports clouds with a negative radiative impact. This mechanism should cause the aforementioned cooling clouds to occur along with high q_{sfc} in the IWVE regions. Given the strength and robustness of the IWVE correlations over several time and spatial scales, this mechanism could have great significance for the heat stress dynamics in the IWVE regions. Although the exact mechanism is not investigated here, we show evidence of such a negative relationship between CRF and q_{sfc} that exists dominantly over the IWVE regions, rendering the 'effective' negative radiative forcing from water vapor.

Over the IWVE regions, we find a robust, significant and large negative (positive) regression between q_{sfc} and daytime CRF (cloud fractional coverage, figure not shown), but insignificant regression between these quantities in the DES regions and positive, insignificant values in some areas of the ITCZ (Fig. 5). This feature of the IWVE, ITCZ and DES regions is observed pan-tropics (Figures 6 and S6) throughout the year (figures not shown). However, we do find the ITCZ regions to have a significant negative correlation between upper tropospheric water vapor and CRF (figure not shown) indicating a dependence of cloud formation on local environmental humidity, as is presumably also the case over the IWVE regions. In the IWVE regions, we however find this strong dependence of CRF on the water vapor present throughout the column (figure not shown). In other words, in the IWVE regions, water vapor in the lower and higher tropospheric levels seems to vary and impact cloud cover in tandem. The mechanism behind this apparent correlation is not understood, however, the correlation enables lower tropospheric water content to be a good indicator of CRF in these regions.

Lastly, the IWVE regions also show a large day-to-day variability in both cloud cover and CRF, which is not present in the DES and ITCZ regions (Fig. 5). Over DES, q_{sfc} is too low to be associated with substantial cloud occurrence, whereas, over the ITCZ it is too high to limit or control the same. While we have not established any cause-and-effect relationships between q_{sfc} and cloud cover in the three regions, the general atmospheric conditions do seem to be less conducive to or supportive of clouds over the DES regions and vice versa over the ITCZ. Some of this possibly could be attributed to the stable conditions that form over the DES regions due to Hadley circulation and vice versa over the ITCZ. The IWVE regions however show a large variability in both q_{sfc} and CRF, suggesting atmospheric conditions variable enough to support different types and amounts of clouds. This feature is observed in most IWVE regions throughout the tropics (figure not shown). The effect of tropical latitudinal overturning circulation on the IWVE regions is analyzed next.

3.4 IWVE co-located with the horizontal branch of Hadley cell - cloudiness not dominated by convective forcing

Cloud formation or occurrence is governed by several factors like water availability and the presence of a vertical lift - either due to buoyancy, low level convergence, turbulence, orography or frontal interaction. As such, a weak control from one factor can give the other processes an upper hand in impacting cloud formation or occurrence. Specifically, the absence of one factor can result in a decrease in a certain type of clouds and favor the other types. The role of a presence or absence of vertical lift on cloud occurrence in the three regions will now be investigated.

An abundant amount of convective forcing is available over the ITCZ throughout the year due to maximum solar insolation, which results in the high cloud cover and precipitation associated with these regions discussed earlier. The divergence of the horizontal wind, column integrated between 500 hPa and 200 hPa in the tropics, shows positive values (divergence) over the ITCZ regions (Fig. 7). Hence, the regions where q_{sfc} is positively (not) correlated with T_{max} (CRF) are also the regions of deep convective forcing. The high cloud cover of all types in these regions supports this inference (Fig. 4). The opposite is true for DES regions which show predominant horizontal convergence, downwelling and clear skies (Fig. 7).

The IWVE regions, on the other hand, are marked by the smallest horizontal divergence and vertical motion as depicted in Figure 7. This is seen by the overlap between the IWVE regions and the contours of near zero divergence of the horizontal winds integrated over the upper troposphere. This feature is present over all IWVE regions in the tropics. This absence of a strong vertical forcing could be related with the dominance of shallow cumulus and altocumulus clouds and the lower areal coverage of deep convective and cirrus clouds in the IWVE regions (Figure 4). It can only be speculated now and verified in a numerical study that vertical forcing is conducive to a certain type of clouds, the absence of which may be related with the IWVE.

3.5 Why could the water vapor indirect effect be important?

The co-location of the IWVE regions with transition cloud cover and negligible vertical motion (or convective forcing) indicate that these regions occur in the horizontal branches of tropical continental scale overturning circulations like the Hadley cell. Clearly, the Hadley cell is not strictly meridionally oriented everywhere, which is why we don't find a strict latitudinal dependence of the IWVE regions over various continents in a given season. In fact, continental scale overturning circulations, like the one found over the northern Sahara in May 2016 (Figure 7), can also engender IWVE regions co-located with their horizontal branches. However, Figure 1 demonstrates clearly that the IWVE is not present in regions between Libya and Mali over a climatological average and may not be important for the regional heat stress climatology. However, in regions affected by a climatological latitudinal overturning circulation, like the Hadley cell, the IWVE could be decisive in determining pre-monsoonal surface heat stress.

To this effect, we provide an example of the surface heat stress during the severe, pan-India heat wave of May 2016. An exhaustive analysis of the general heat stress at these latitudes, their relation with the IWVE and any deviations will be presented in a follow up study. India lies in the Southeast Asian belt where both high temperature and high humidity contribute significantly to heat stress (Im et al., 2017; Hoegh-Guldberg et al., 2018; Wehner et al., 2016) particularly in April, May and June. While IWVE shows an inverse relationship between these variables, their combination could be above the extreme heat wave threshold, as shown by Wehner et al. (2016) for May 2015 in Hyderabad, India. Hence, this region has been chosen for a case study. Record high near surface temperatures of 51 degrees were observed in Phalodi, Rajasthan (27.13°N, 72.36°E) around 19^{th} May 2016 with the heat wave impacting regions pan-India between the months of April and June (Agarwal, 2016; Wu, 2016; Mazdiyasni et al., 2017; Oldenborgh et al., 2018). The impact of this heat wave on human health was severe as evidenced by a high number of newspaper reports on heat strokes and human fatalities in this period (Tharoor, 2016). We present a preliminary meteorological analysis of this heat wave to show a possible relevance of the IWVE during the heat wave period.

Sources of tropical heat stress are not as well understood as are for their extra-tropical counterparts (Perkins, 2015). For example, there are only a handful of studies which apply the 'blocking high' theory of heat waves to these latitudes (Rohini et al., 2016; Ratnam et al., 2016; Oueslati et al., 2017). We endeavor to show through this analysis that the IWVE, identified in the months of April, May and June over the subcontinent, may also explain a significant portion of the general surface temperature variability, sometimes even during the maximum heat wave period. At this point, following previous modeling studies, it is noted that at around 25° latitude, heat waves associated with extreme geopotential anomalies may take effect only in a couple of days as compared to almost a week at higher latitudes (Jiménez-Esteve & Domeisen, 2022; Lau & Nath, 2014). Also the maximum in T_{max} is found to be co-eval with the maximum in the geopotential height anomaly (ΔGH) (Jiménez-Esteve & Domeisen, 2022). That is, any lag, of the extreme T_{max}, more than a couple of days from the development of statistically significant positive ΔGH may be indicative of other controlling processes. These studies also show that at 25° latitude, the mid tropospheric ΔGH associated with heat waves could be around 30 m, which can increase to up to 100 m at higher latitudes.

Figure 8 shows the May 2016 time series of several meteorological variables over Phalodi, Rajasthan, India. The variables q_z, pressure velocity at 550 hPa (ω_{550}) and CRF derived from ERA5, averaged over a 2°×2° region centered around Phalodi are used to understand the IWVE. Following studies of extra-tropical heat waves, the geopotential height anomalies from a climatological mean (1979 to 2020) at 800 hPa and 550 hPa (ΔGH_{800}, ΔGH_{550}) are used to represent the role of blocking highs in triggering heat stress. Figure S7 shows the same variables over other regions in the subcontinent during the same heat wave. These regions were chosen because they have either a high IWVE, ΔT_{max} or ΔGH_{550} signal. These figures are summarised in Table 1.

The IWVE correlations, either with q_{sfc} or with CWV are moderately high and statistically significant for all stations during May 2016. The correlation between T_{max} and GH_{550} is smaller and mostly insignificant at all stations. The highest T_{max} anomalies appear around 17^{th} to 19^{th} May, except in Dachepalli in eastern India. The onset of significant ΔT_{max} usually lags significant ΔGH_{550} by around 4-7 days at all stations except Dachepalli where the heat wave starts right after a period of heavy precipitation. Except for Phalodi, no station has a significant ΔGH_{550} on the day of the maxima in T_{max}. But, for Phalodi, although the period of maximum T_{max} is co-eval with a significant ΔGH_{550}, the maxima in ΔGH_{550} occurs 10 days earlier. Some stations like Lucknow and Maharashtra don't show a persistent multi-day positive ΔGH_{550} preceding or co-eval with the heat wave. In most cases, the period of significant positive ΔGH_{550} or ΔT_{max} are not associated with statistically significant downwelling. However, during the period of significant ΔT_{max} the CRF is, in general, low in magnitude as compared to the rest of the month or even maximum positive for Gujarat during this period. The rest of the month is marked by larger negative CRF in general. It is noteworthy that this period of low CRF does not coincide with the period of significant positive ΔGH_{550}.

The above preliminary analysis suggests that statistically significant geopotential anomalies are not co-eval with the period of highest heat stress at least over the Indian subcontinent during the severe heat wave of May 2016. In fact, these periods may be separated from each other by several days. At the same time, every station is found to be significantly impacted by the IWVE, especially during extremes in surface temperatures. This observation, although does not preclude the possible role of a blocking high in impacting the heat wave, does provide support for the role of the tropics-wide IWVE in causing regular heat stress throughout the pre-monsoon summer season, every year, contiguously throughout the tropics. This is observed in the Indian subcontinent, which regularly experiences pre-monsoon heat stress (Pai et al., 2013), which could have a dominant component from the continuously varying humidity resulting in extremes in temperature.

It should be noted that May 2016 was a severe pre-monsoon heat stress year for the Indian subcontinent, hence the atmosphere could be impacted by certain synoptic scale conditions, other than the IWVE, not considered in detail here. Moreover, this analysis does not consider positive feedback from dry soils which might add another layer of complexity to local T_{max} evolution (Miralles et al., 2014; Perkins, 2015). Hence, further investigation is needed to unravel the relative significance of these processes in causing heat stress at these latitudes.

4 Conclusion

This study shows the existence of regions at the borders of the inter-tropical convergence zone where the atmospheric dynamics seems to specifically support the occurrence of clouds with a negative radiative impact on daily maximum surface temperatures T_{max} in the current climate. Additionally, other clouds, known to have a positive radiative forcing, have tapering down occurrences in these same regions. Both, cloud areal coverage and surface cloud radiative forcing (CRF) have a positive correlation with lower tropospheric water vapor q_{sfc} in these regions. As a result, surface temperatures are strongly negatively correlated with water vapor. These regions, where water vapor has an apparent negative impact on surface warming, have been referred to as the regions of 'indirect water vapor effect' or IWVE.

Such a negative forcing from water vapor is not observed in any other extensive region outside this belt around the ITCZ which coincides with the horizontal branch of latitudinal overturning circulations, like the Hadley cell. The negative daily CRF may not be unique to the IWVE regions, however the strong positive correlation of q_{sfc} with CRF and negative correlation in turn with T_{max} is uniquely observed in the IWVE regions only. We suspect that in other regions, processes other than IWVE which impact T_{max} through q_{sfc}, may become important, but were not the focus of this study. The mechanism which lets water vapor to be dominantly, positively correlated with cloud occurrence of low and mid-level clouds in these regions, remains to be explored.

The IWVE regions occur on both sides of the ITCZ in all seasons and follow its annual north-to-south march. This means, periods where IWVE is active, both precede and succeed the monsoon in a tropical region. Although not addressed in detail in this study, this can have consequences for pre-monsoonal heat stress in regions like the Sahel in Africa, the Cerrado in South America and the Indian subcontinent where the IWVE is found active in this season which is already fraught with positive surface temperature feedback from receding soil moisture (Perkins, 2015; Pai et al., 2013; Miralles et al., 2014; Oueslati et al., 2017). The post monsoon occurrence of the IWVE may not have a substantial health impact because of the general lower surface temperatures due to wet soils and a receding sun after the monsoons. An in-depth analysis of the role of IWVE versus other mechanisms of pre-monsoon heat stress in these regions is required.

Lastly, The IWVE seems to have a connection with the horizontal branch of latitudinal overturning circulations in the tropics, in the way the latter affects cloud distribution. With evidence that tropical overturning circulations, like the Hadley cell, are set to change in a warmer climate (Lu et al., 2007), the IWVE and its associated impact on surface temperatures may evolve as well. An understanding of how this sensitive balance would be modified under global climate change could be important, especially because in the IWVE regions, this effect may be substantially associated with pre-monsoonal heat stress.

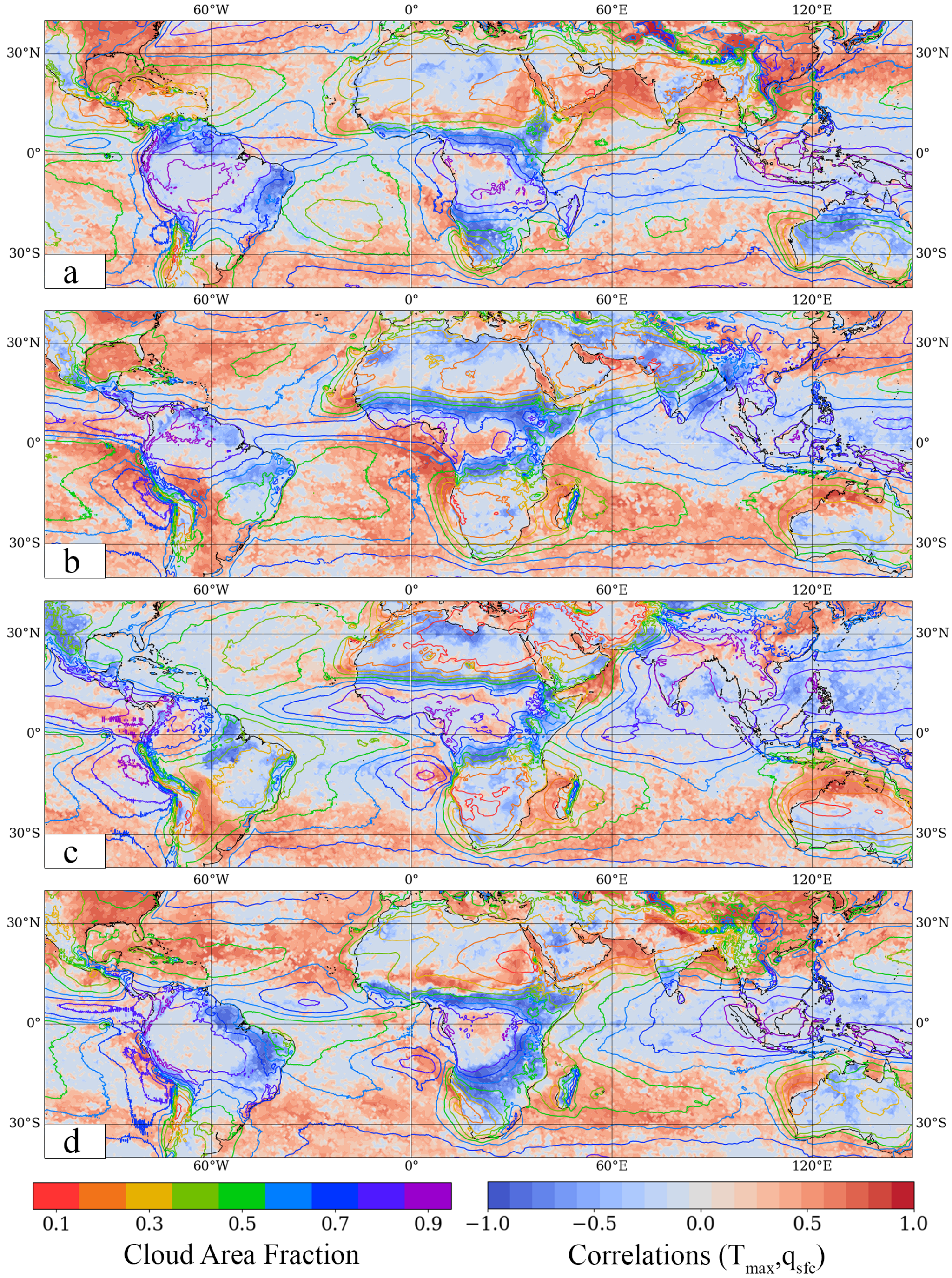

Figure 1. The tropical indirect water vapor negative radiative effect and its co-occurrence with transition regions in cloud fraction. Colored Shading - Mode of monthly daily scale correlations between daily T_{max} and q_{sfc} in (a) February, (b) May, (c) August, and (d) November. The mode was calculated from the population of all monthly correlations between 2001-2020. See methods for details. Colored line Contours – Average total cloud area fraction for the corresponding months between 2001 and 2020. All data from ERA5.

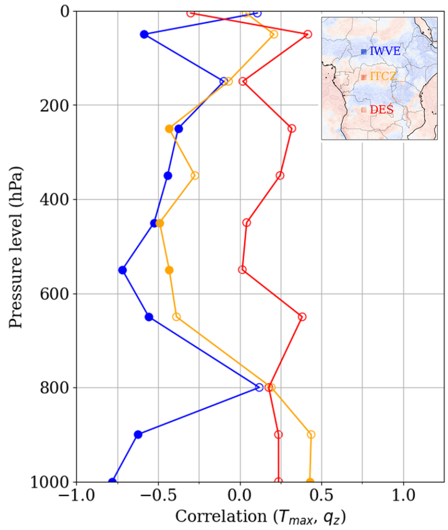

Figure 2. IWVE regions show negative correlations between T_{max} and upper tropospheric specific humidity. Correlation coefficients between daily T_{max} and daily average specific humidity at various altitudes, q_z, in May 2016 at selected IWVE, ITCZ and DES regions in Africa (inset). Data from ERA5. Correlations significant at the 95% confidence level are shown with filled circles.

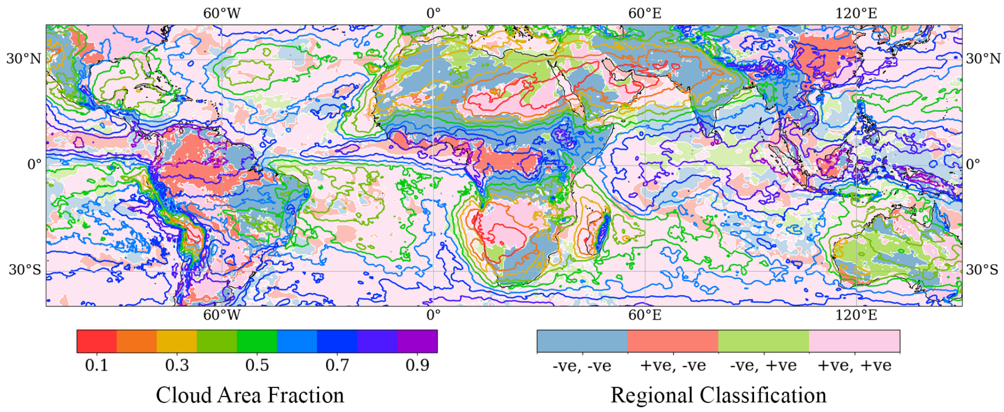

Figure 3. Dominant IWVE regions in the tropics. Classification of various regions into four types based on whether the sign of the grid scale correlations between daily T_{max} and q_{sfc} is the same as that between T_{max} and CWV. Area 1 - both negative, Area 2 - former positive, latter negative, Area 3 - negative, positive, Area 4 - both positive. Data obtained from ERA5 for May 2016 (compare this with Figure S1b). The map has an overlay of average cloud cover for May 2016. Ocean grid points have been de-saturated.

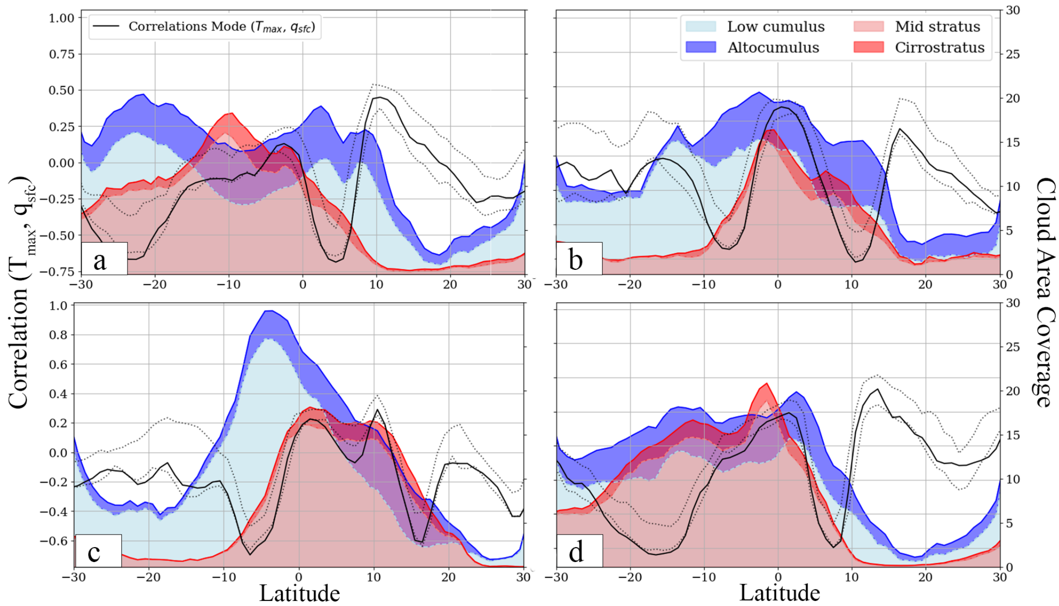

Figure 4. Dominant presence of mid level clouds in IWVE regions. Daytime cloud fraction over Africa, zonally averaged between 30°N, 17.5°E and 30°S, 30°E for (a) February, (b) May, (c) August, and (d) November, 2001 to 2020. Could types shown - Low cumulus including shallow cumulus (low, thin) and stratocumuls (low, medium thick); altocumulus (mid, thin); mid stratus including altostratus (mid, medium thickness) and nimbostratus (mid, thick); cirrostratus (high, medium thick). Data from CERES CldTypHist 1°×1° monthly average day time values. Cumulus and stratus clouds with the largest % area coverage have been shown, while other cloud species such as deep convection, nimbostratus and cirrus clouds have been omitted from this analysis due to their comparatively low area coverage (see Fig. S5). This is done assuming that clouds with small % area cover do not have dominant radiative effect at the surface.

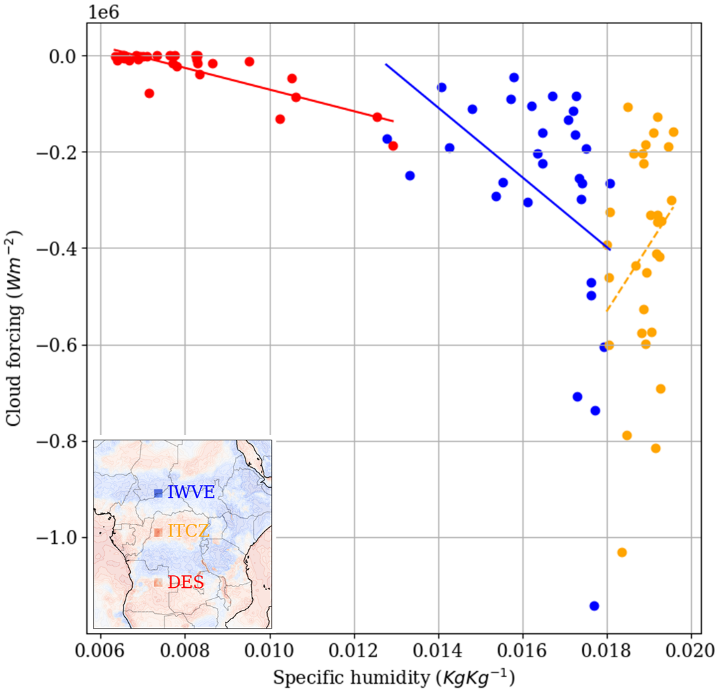

Figure 5. Surface cloud radiative forcing in IWVE regions is sensitive to near surface atmospheric humidity. Daytime averaged CRF versus q_{sfc} for a $1° \times 1°$ IWVE, ITCZ and a DES region in Africa (inset), for all days in May 2016. All data from ERA5.

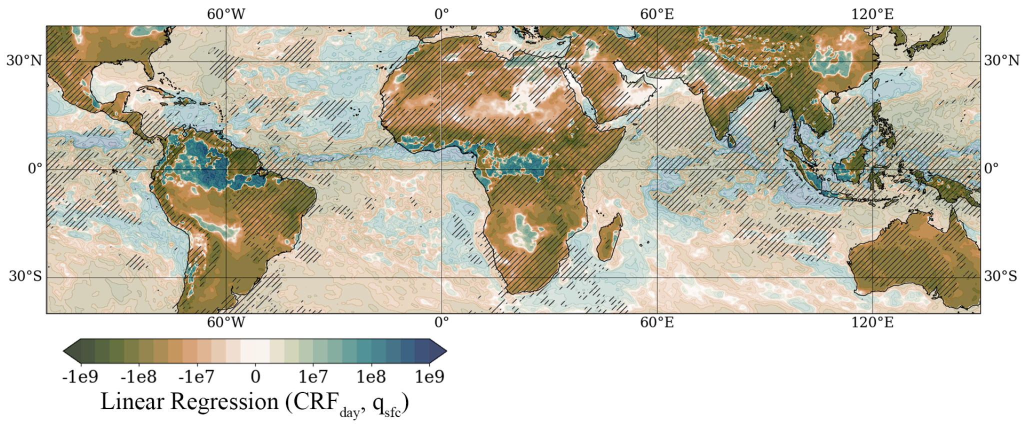

Figure 6. IWVE across tropics show a negative relation of surface humidity with cloud radiative forcing. Coefficients of linear regression of daytime CRF on daily averaged q_{sfc}. Regression performed with ERA5 grid scale, daily data for May 2016. Most values above -7e7 are significant at the 95% confidence level. Most positive regression coefficients are insignificant. Statistical significance is not shown to improve figure clarity. Hatching shows all regions with negative correlations between T_{max} and q_{sfc}. Data obtained from ERA5.

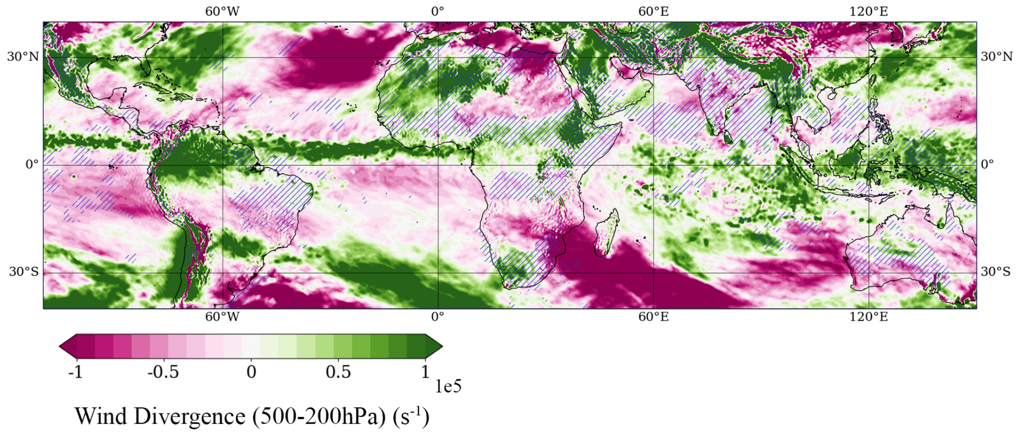

Figure 7. IWVE associated with the horizontal branch of continental scale overturning circulations. Shading shows the divergence of horizontal winds, column integrated between 500 hPa and 200 hPa averaged over May 2016. Hatching shows IWVE regions with T_{max}, q_{sfc} correlation coefficients between -1 and -0.5. Data obtained from ERA5.

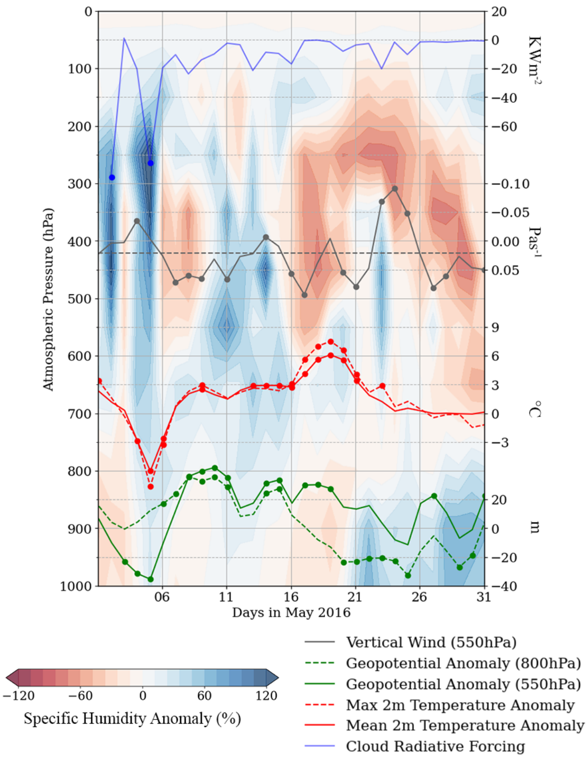

Figure 8. Severe tropical heat stress could be related to IWVE. Daily scale time series of T_{max}, T_{avg} (daily mean), GH_{800} and GH_{550} anomalies from the climatological mean corresponding to May 1979 to 2020. Figure also shows the percentage temporal anomalies in q_z from the monthly mean of May 2016, the daytime CRF and daily 550 hPa vertical wind ω_{550}. The dashed grey line represents the climatological average vertical wind in May. Significant anomalies are marked. Significant differences of CRF and ω_{550} from the monthly and climatological mean respectively are also marked. All variables derived from a 2°×2° area over Phalodi, north-western India in May 2016. Data obtained from ERA5.

Table 1. Importance of IWVE during the heat wave of May 2016 over the Indian subcontinent. Meteorological conditions during the May 2016 heat wave recorded in India. Statistics calculated using a month long daily scale time series of meteorological variables around centers of heat stress, with the same methodology as used in Figure 8. Meteorological conditions for two types of days are analyzed - day of the monthly maximum T_{max} and the day of the monthly maximum geopotential anomaly at 550 hPa, ΔGH_{550}. For the heat wave day values are reported for the daily maximum and averaged surface temperature anomalies from the climatological (1979 to 2020) monthly mean ΔT_{max} and ΔT_{avg}, daily scale IWVE correlations corr(T_{max},q_{sfc}) and corr(T_{max},CWV), daily scale area averaged vertical wind at 550 hPa ω_{550}, daytime averaged surface CRF, anomaly in the geopotential heights at the 800 hPa and 550 hPa levels during the heat wave period (ΔGH_{800}, ΔGH_{550}), and correlations corr(T_{max},GH_{800}) and corr(T_{max},GH_{550}). Some of these values are also reported for the day of maximum ΔGH_{550}. Statistics significant at the 95% confidence level are bold. All data from ERA5. All values are averaged over a 2°×2° area around the region under study.

	Phalodi	Datia	Lucknow	Dachepalli	Radhanpur	Patoda
latitude (°N)	27.13	25.67	26.87	16.5	23.75	18.75
longitude (°E)	72.36	78.45	80.94	79.75	71.75	75.5
avg($T_{avg,May}$)	34.96	34.05	33.78	33.2	33.7	32.38
Day of max(T_{max})	19	18	17	24	18	17
ΔT_{max} (°C)	**7.51**	**3.97**	**4.26**	**4.16**	**6.14**	**3.79**
ΔT_{avg} (°C)	**6.1**	**3.83**	**3.54**	**4.05**	**3.99**	**3.8**
corr(T_{max},q_{sfc})	**-0.4**	**-0.37**	**-0.47**	**-0.81**	**-0.37**	**-0.45**
corr(T_{max},CWV)	**-0.62**	**-0.41**	**-0.57**	**-0.67**	**-0.69**	-0.24
ω_{550} (Pa sec^{-1})	0.0	0.0	0.01	**0.03**	0.03	0.03
CRF (kW m^{-2})	-1.51	0	-19.1	-33.39	0.5	-18.97
ΔGH_{800} (m)	-13.16	-14.83	-11.04	3.86	-10.91	**-20.2**
ΔGH_{550} (m)	**27.6**	14.37	6.27	7.62	**19.74**	-2.96
corr(T_{max},GH_{800})	-0.2	**-0.39**	-0.17	0.33	0	-0.13
corr(T_{max},GH_{550})	**0.38**	0.17	0.32	**0.39**	**0.4**	0.31
Day of max(ΔGH_{550})	10	14	14	14	14	14
ΔT_{max} (°C)	2.27	**2.73**	**3.11**	1.01	**2.43**	**2.38**
ΔGH_{550} (m)	**42.33**	**35.53**	**35.22**	**29.9**	**32.01**	**34.9**
CRF (kW m^{-2})	-9.98	-31.9	-30.56	-22.33	0.28	-76.91

5 Open Research

[H] The meteorological data used for the heat stress analysis in the study is available freely on the Copernicus Climate Data Store via 10.24381/cds.143582cf, `https://cds.climate.copernicus.eu/#!/search?text=ERA5&type=dataset` (Hersbach et al., 2020, 2023). Supporting meteorological data from the AIRS L3 standard data products V7 is obtained from the data collections at NASA GES DISC via 10.5067/UO3Q64CTTS1U, `https://disc.gsfc.nasa.gov/datasets?page=1&source=AQUA%20AIRS&keywords=airs%20version%207` (AIRS, 2019). CERES cloud type and surface radiation flux data are obtained from the SYN1deg level 3 products from the NASA CERES data repository via (doi - 10.5067/TERRA+AQUA/CERES/CLDTYPHIS_L3.004, doi - 10.5067/Terra+Aqua/CERES/SYN1degDay_L3.004A respectively) `https://ceres.larc.nasa.gov/data/` (Doelling et al., 2013, 2016). All datasets used are available freely for public use.

All original Python (> 3.9) code will be archived if the manuscript is accepted and can be obtained from the repository or upon request from Karan at karan42mahajan@gmail.com. All data used from the above sources can also be separately obtained from Karan.

Acknowledgments

The authors acknowledge financial support from the National Institute of Science Education and Research, Bhubaneshwar, India and the Ministry of Education, Government of India, grant number MoE-STARS1/766.

References

Agarwal, V. (2016, 5). Indian heat wave breaks record for highest temperature. *The Wall Street Journal*. Retrieved from `https://www.wsj.com/articles/BL-IRTB-32135`

AIRS. (2019). *Airs project, aqua/airs l3 daily standard physical retrieval (airs-only) 1 degree x 1 degree v7.0 [dataset]*. doi: 10.5067/UO3Q64CTTS1U

Alizadeh, M. R., Abatzoglou, J. T., Adamowski, J. F., Prestemon, J. P., Chittoori, B., Asanjan, A. A., & Sadegh, M. (2022, 2). Increasing heat-stress inequality in a warming climate. *Earth's Future*, *10*. doi: 10.1029/2021EF002488

Allan, R. P., Shine, K. P., Slingo, A., & Pamment, J. A. (1999, 7). The dependence of clear-sky outgoing long-wave radiation on surface temperature and relative humidity. *Quarterly Journal of the Royal Meteorological Society*, *125*, 2103-2126. doi: 10.1002/qj.49712555809

Araújo, I., Marimon, B. S., Scalon, M. C., Fauset, S., Marimon, B. H., Tiwari, R., ... Gloor, M. U. (2021, 3). Trees at the amazonia-cerrado transition are approaching high temperature thresholds. *Environmental Research Letters*, *16*. doi: 10.1088/1748-9326/abe3b9

Biemans, H., Siderius, C., Mishra, A., & Ahmad, B. (2016, 5). Crop-specific seasonal estimates of irrigation-water demand in south asia. *Hydrology and Earth System Sciences*, *20*, 1971-1982. doi: 10.5194/hess-20-1971-2016

Bouniol, D., Couvreux, F., Kamsu-Tamo, P. H., Leplay, M., Guichard, F., Favot, F., & O'connor, E. J. (2012, 3). Diurnal and seasonal cycles of cloud occurrences, types, and radiative impact over west africa. *Journal of Applied Meteorology and Climatology*, *51*, 534-553. doi: 10.1175/JAMC-D-11-051.1

Bourgeois, Q., Ekman, A. M., Igel, M. R., & Krejci, R. (2016, 8). Ubiquity and impact of thin mid-level clouds in the tropics. *Nature Communications*, *7*. doi: 10.1038/ncomms12432

Brutsaert, W. (1975, 10). On a derivable formula for long-wave radiation from clear skies. *Water Resources Research*, *11*, 742-744. doi: 10.1029/WR011i005p00742

Carmona, F., Rivas, R., & Caselles, V. (2014). Estimation of daytime downward longwave radiation under clear and cloudy skies conditions over a sub-humid region. *Theoretical and Applied Climatology*, *115*, 281-295. doi: 10.1007/s00704-013-0891-3

Chen, T., Rossow, W. B., & Zhang, Y. (2000, 1). Radiative effects of cloud-type variations. *Journal of Climate*, *13*, 264-286. doi: 10.1175/1520-0442(2000)013⟨0264:REOCTV⟩2.0.CO;2

Coffel, E. D., Horton, R. M., & Sherbinin, A. D. (2018, 1). Temperature and humidity based projections of a rapid rise in global heat stress exposure during the 21st century. *Environmental Research Letters*, *13*. doi: 10.1088/1748-9326/aaa00e

Coumou, D., Robinson, A., & Rahmstorf, S. (2013). Global increase in record-breaking monthly-mean temperatures. *Climatic Change*, *118*, 771-782. doi: 10.1007/s10584-012-0668-1

Derbyshire, S., Beau, I., Bechtold, P., Grandpeix, J.-Y., Piriou, J.-M., Redelsperger, J.-L., & Soares, P. (2004, 10). Sensitivity of moist convection to environmental humidity. *Quarterly Journal of the Royal Meteorological Society*, *130*, 3055-3079. doi: 10.1256/qj.03.130

de Rooy, W. C., Bechtold, P., Fröhlich, K., Hohenegger, C., Jonker, H., Mironov, D., ... Yano, J. I. (2013, 1). Entrainment and detrainment in cumulus convection: An overview. *Quarterly Journal of the Royal Meteorological Society*, *139*, 1-19. doi: 10.1002/qj.1959

Dessler, A. E., Schoeberl, M. R., Wang, T., Davis, S. M., & Rosenlof, K. H. (2013, 11). Stratospheric water vapor feedback. *Proceedings of the National Academy of Sciences of the United States of America*, *110*, 18087-18091. doi: 10.1073/pnas.1310344110

Doelling, D. R., Loeb, N. G., Keyes, D. F., Nordeen, M. L., Morstad, D., Nguyen, C., ... Sun, M. (2013, 6). Geostationary enhanced temporal interpolation for ceres flux products [dataset]. *Journal of Atmospheric and Oceanic Technology*, *30*, 1072-1090. doi: 10.1175/JTECH-D-12-00136.1

Doelling, D. R., Sun, M., Nguyen, L. T., Nordeen, M. L., Haney, C. O., Keyes, D. F., & Mlynczak, P. E. (2016, 3). Advances in geostationary-derived longwave fluxes for the ceres synoptic (syn1deg) product [dataset]. *Journal of Atmospheric and Oceanic Technology*, *33*, 503-521. doi: 10.1175/JTECH-D-15-0147.1

Douglas, E. M., Beltrán-Przekurat, A., Niyogi, D., Pielke, R. A., & Vörösmarty, C. J. (2009, 5). The impact of agricultural intensification and irrigation on land-atmosphere interactions and indian monsoon precipitation - a mesoscale modeling perspective. *Global and Planetary Change*, *67*, 117-128. doi: 10.1016/j.gloplacha.2008.12.007

Douglas, E. M., Niyogi, D., Frolking, S., Yeluripati, J. B., Pielke, R. A., Niyogi, N., ... Mohanty, U. C. (2006). Changes in moisture and energy fluxes due to agricultural land use and irrigation in the indian monsoon belt. *Geophysical Research Letters*, *33*. doi: 10.1029/2006GL026550

Dunne, J. P., Stouffer, R. J., & John, J. G. (2013, 6). Reductions in labour capacity from heat stress under climate warming. *Nature Climate Change*, *3*, 563-566. doi: 10.1038/nclimate1827

Findell, K. L., & Eltahir, E. A. B. (2003a). Atmospheric controls on soil moisture-boundary layer interactions. part i: Framework development. *Journal of Hydrometeorology*, *4*, 552-569. doi: 10.1175/1525-7541(2003)004⟨0552:acosml⟩2.0.co;2

Findell, K. L., & Eltahir, E. A. B. (2003b, 6). Atmospheric controls on soil moisture–boundary layer interactions. part ii: Feedbacks within the continental united states. *Journal of Hydrometeorology*, *4*, 570-583. doi: 10.1175/1525-7541(2003)004⟨0570:ACOSML⟩2.0.CO;2

Flerchinger, G. N., Xaio, W., Marks, D., Sauer, T. J., & Yu, Q. (2009, 3). Comparison of algorithms for incoming atmospheric long-wave radiation. *Water Resources Research*, *45*. doi: 10.1029/2008WR007394

Forster, P., Storelvmo, T., Armour, K., Collins, W., Dufresne, J.-L., Frame, D., ... Zhang, H. (2021, 7). The earth's energy budget, climate feedbacks and climate sensitivity. In (p. 923-1054). Cambridge University Press. Retrieved from `https://www.cambridge.org/core/product/identifier/9781009157896%23c7/type/book_part` doi: 10.1017/9781009157896.009

Gaffen, D. J., Elliott, W. P., & Robock, A. (1992, 9). Relationships between tropospheric water vapor and surface temperature as observed by radiosondes. *Geophysical Research Letters*, *19*, 1839-1842. doi: 10.1029/92GL02001

Hartmann, D. L., Ockert-Bell, M. E., & Michelsen, M. L. (1992, 11). The effect of cloud type on earth's energy balance: Global analysis. *Journal of Climate*, *5*, 1281-1304. doi: 10.1175/1520-0442(1992)005⟨1281:TEOCTO⟩2.0.CO;2

Hersbach, H., Bell, B., Berrisford, P., Biavati, G., Horányi, A., Sabater, J. M., ... Thépaut, J.-N. (2023). *Era5 hourly data on pressure levels from 1940 to present [dataset].* doi: https://doi.org/10.24381/cds.bd0915c6

Hersbach, H., Bell, B., Berrisford, P., Hirahara, S., Horányi, A., Muñoz-Sabater, J., ... Thépaut, J. (2020, 7). The era5 global reanalysis [dataset]. *Quarterly Journal of the Royal Meteorological Society*, *146*, 1999-2049. doi: 10.1002/qj.3803

Hoegh-Guldberg, O., Jacob, D., Taylor, M., Bindi, M., Brown, S., Camilloni, I., ... Zhou, G. (2018). *Impacts of 1.5 ºc global warming on natural and human systems global warming of 1.5°c. an ipcc special report on the impacts of global warming of 1.5°c above pre-industrial levels and related global greenhouse gas emission pathways, in the context of strengthening the global response to the threat of climate change, sustainable development, and efforts to eradicate poverty, ipcc.*

Holloway, C. E., Neelin, J. D., Holloway, C. E., & Neelin, J. D. (2009, 6). Moisture vertical structure, column water vapor, and tropical deep convection. *Journal of the Atmospheric Sciences*, *66*, 1665-1683. doi: 10.1175/2008JAS2806.1

Im, E. S., Pal, J. S., & Eltahir, E. A. (2017, 8). Deadly heat waves projected in the densely populated agricultural regions of south asia. *Science Advances*, *3*. doi: 10.1126/sciadv.1603322

IMD. (2002, 2). *Recommendation regarding the revised criteria for declaring heat wave/ cold wave, ddgm (wf).*

Iwasa, Y., Arakawa, T., & Sumi, A. (2012). Tropospheric mid-level detrainment flow obtained from high-resolution non-hydrostatic atmospheric model experiments. *Journal of the Meteorological Society of Japan. Ser. II*, *90*, 11-33. doi: 10.2151/jmsj.2012-102

Jiménez-Esteve, B., & Domeisen, D. I. (2022, 7). The role of atmospheric dynamics and large-scale topography in driving heatwaves. *Quarterly Journal of the Royal Meteorological Society*, *148*, 2344-2367. doi: 10.1002/qj.4306

Johnson, R. H., Ciesielski, P. E., & Hart, K. A. (1996, 7). Tropical inversions near the 0°c level. *Journal of the Atmospheric Sciences*, *53*, 1838-1855. doi: 10.1175/1520-0469(1996)053⟨1838:TINTL⟩2.0.CO;2

Johnson, R. H., Rickenbach, T. M., Rutledge, S. A., Ciesielski, P. E., & Schubert, W. H. (1999). *Trimodal characteristics of tropical convection.*

Lau, N.-C., & Nath, M. J. (2014, 5). Model simulation and projection of european heat waves in present-day and future climates. *Journal of Climate*, *27*, 3713-3730. doi: 10.1175/JCLI-D-13-00284.1

Lawston, P. M., Santanello, J. A., Hanson, B., & Arsensault, K. (2020). Impacts of irrigation on summertime temperatures in the pacific northwest. *Earth Interactions d*, *24*. doi: 10.1175/EI-D-19-0015.s1

Li, D., Yuan, J., & Kopp, R. E. (2020, 6). Escalating global exposure to compound heat-humidity extremes with warming. *Environmental Research Letters*, *15*.

doi: 10.1088/1748-9326/ab7d04

Li, M., Liao, Z., & Coimbra, C. F. (2018, 4). Spectral model for clear sky atmospheric longwave radiation. *Journal of Quantitative Spectroscopy and Radiative Transfer*, *209*, 196-211. doi: 10.1016/j.jqsrt.2018.01.029

Li, X. X. (2020, 6). Heat wave trends in southeast asia during 1979–2018: The impact of humidity. *Science of the Total Environment*, *721*. doi: 10.1016/j.scitotenv.2020.137664

Lobell, D. B., & Bonfils, C. (2008, 5). The effect of irrigation on regional temperatures: A spatial and temporal analysis of trends in california, 1934-2002. *Journal of Climate*, *21*, 2063-2071. doi: 10.1175/2007JCLI1755.1

Lobell, D. B., Bonfils, C., & Faurès, J. M. (2008). The role of irrigation expansion in past and future temperature trends. *Earth Interactions*, *12*. doi: 10.1175/2007EI241.1

Lu, J., Vecchi, G. A., & Reichler, T. (2007, 3). Expansion of the hadley cell under global warming. *Geophysical Research Letters*, *34*, L06805. doi: 10.1029/2006GL028443

Mahlstein, I., Knutti, R., Solomon, S., & Portmann, R. W. (2011). Early onset of significant local warming in low latitude countries. *Environmental Research Letters*, *6*. doi: 10.1088/1748-9326/6/3/034009

Mazdiyasni, O., AghaKouchak, A., Davis, S. J., Madadgar, S., Mehran, A., Ragno, E., ... Niknejad, M. (2017, 6). Increasing probability of mortality during indian heat waves. *Science Advances*, *3*. doi: 10.1126/sciadv.1700066

Miralles, D. G., Teuling, A. J., Heerwaarden, C. C. V., & Arellano, J. V. G. D. (2014). Mega-heatwave temperatures due to combined soil desiccation and atmospheric heat accumulation. *Nature Geoscience*, *7*, 345-349. doi: 10.1038/ngeo2141

Oldenborgh, G. J. V., Philip, S., Kew, S., Weele, M. V., Uhe, P., Otto, F., ... Achutarao, K. (2018, 1). Extreme heat in india and anthropogenic climate change. *Natural Hazards and Earth System Sciences*, *18*, 365-381. doi: 10.5194/nhess-18-365-2018

Oueslati, B., Pohl, B., Moron, V., Rome, S., & Janicot, S. (2017, 5). Characterization of heat waves in the sahel and associated physical mechanisms. *Journal of Climate*, *30*, 3095-3115. doi: 10.1175/JCLI-D-16-0432.1

Pai, D. S., Nair, A., & Ramanathan, A. N. (2013). *Long term climatology and trends of heat waves over india during the recent 50 years (1961-2010)* (Vol. 64).

Parker, D. J., Willetts, P., Birch, C., Turner, A. G., Marsham, J. H., Taylor, C. M., ... Martin, G. M. (2016, 7). The interaction of moist convection and mid-level dry air in the advance of the onset of the indian monsoon. *Quarterly Journal of the Royal Meteorological Society*, *142*, 2256-2272. doi: 10.1002/qj.2815

Perkins, S. E. (2015, 10). *A review on the scientific understanding of heatwaves-their measurement, driving mechanisms, and changes at the global scale* (Vol. 164-165). Elsevier Ltd. doi: 10.1016/j.atmosres.2015.05.014

Puma, M. J., & Cook, B. I. (2010). Effects of irrigation on global climate during the 20th century. *Journal of Geophysical Research Atmospheres*, *115*. doi: 10.1029/2010JD014122

Ramanathan, V., Cess, R. D., Harrison, E. F., Minnis, P., Barkstrom, B. R., Ahmad, E., & Hartmann, D. (1989, 1). Cloud-radiative forcing and climate: Results from the earth radiation budget experiment. *Science*, *243*, 57-63. doi: 10.1126/science.243.4887.57

Ratnam, J. V., Behera, S. K., Ratna, S. B., Rajeevan, M., & Yamagata, T. (2016, 4). Anatomy of indian heatwaves. *Scientific Reports*, *6*. doi: 10.1038/srep24395

Reich, P. B., Sendall, K. M., Rice, K., Rich, R. L., Stefanski, A., Hobbie, S. E., & Montgomery, R. A. (2015, 1). Geographic range predicts photosynthetic and growth response to warming in co-occurring tree species. *Nature Climate*

Change, *5*, 148-152. doi: 10.1038/nclimate2497

Riihimaki, L. D., Mcfarlane, S. A., & Comstock, J. M. (2012, 10). Climatology and formation of tropical midlevel clouds at the darwin arm site. *Journal of Climate*, *25*, 6835-6850. doi: 10.1175/JCLI-D-11-00599.1

Rohini, P., Rajeevan, M., & Srivastava, A. K. (2016, 5). On the variability and increasing trends of heat waves over india. *Scientific Reports*, *6*. doi: 10.1038/srep26153

Ross, R. J., Elliott, W. P., Seidel, D. J., & Grou, P. A.-I. M. (2002, 2). Lower-tropospheric humidity–temperature relationships in radiosonde observations and atmospheric general circulation models. *Journal of Hydrometeorology*, *3*, 26-38. doi: 10.1175/1525-7541(2002)003⟨0026:LTHTRI⟩2.0.CO;2

Schiro, K. A., Neelin, J. D., Adams, D. K., & Lintner, B. R. (2016). Deep convection and column water vapor over tropical land versus tropical ocean: A comparison between the amazon and the tropical western pacific. *Journal of the Atmospheric Sciences*, *73*, 4043-4063. doi: 10.1175/jas-d-16-0119.1

Shakespeare, C. J., & Roderick, M. L. (2021, 10). The clear-sky downwelling longwave radiation at the surface in current and future climates. *Quarterly Journal of the Royal Meteorological Society*, *147*, 4251-4268. doi: 10.1002/qj.4176

Soden, B. J., Jackson, D. L., Ramaswamy, V., Schwarzkopf, M. D., & Huang, X. (2005, 11). The radiative signature of upper tropospheric moistening. *Science*, *310*, 841-844. doi: 10.1126/science.1115602

Soden, B. J., Wetherald, R. T., Stenchikov, G. L., & Robock, A. (2002, 4). Global cooling after the eruption of mount pinatubo: A test of climate feedback by water vapor. *Science*, *296*, 727-730. doi: 10.1126/science.296.5568.727

Stein, T. H., Parker, D. J., Delanoë, J., Dixon, N. S., Hogan, R. J., Knippertz, P., . . . Marsham, J. H. (2011). The vertical cloud structure of the west african monsoon: A 4 year climatology using cloudsat and calipso. *Journal of Geophysical Research Atmospheres*, *116*. doi: 10.1029/2011JD016029

Tharoor, I. (2016, 4). Brutal heat wave in india puts 330 million people at risk. *Washington Post*.

Tiwari, R., Gloor, E., da Cruz, W. J. A., Marimon, B. S., Marimon-Junior, B. H., Reis, S. M., . . . Galbraith, D. (2021, 7). Photosynthetic quantum efficiency in south-eastern amazonian trees may be already affected by climate change. *Plant Cell and Environment*, *44*, 2428-2439. doi: 10.1111/pce.13770

Wehner, M., Stone, D., Krishnan, H., AchutaRao, K., & Castillo, F. (2016). The deadly combination of heat and humidity in india and pakistan in summer 2015. *Bulletin of the American Meteorological Society*, *97*, S81–S86. doi: 10.1175/Bams-D-16-0145.1

Wu, H. (2016, 5). Mercury rising: India records its highest temperature ever. *Cable News Network*.

Supporting Information for "An indirect, negative radiative effect of water vapor in the tropics and its implications for regional surface heat stress"

J. Khanna[1,2], Karan[1,2]

[1]School of Earth and Planetary Sciences, National Institute of Science Education and Research, Jatni, 752050, India

[2]Homi Bhabha National Institute, Training School Complex, Anushaktinagar, Mumbai, 400094, India

Contents of this file

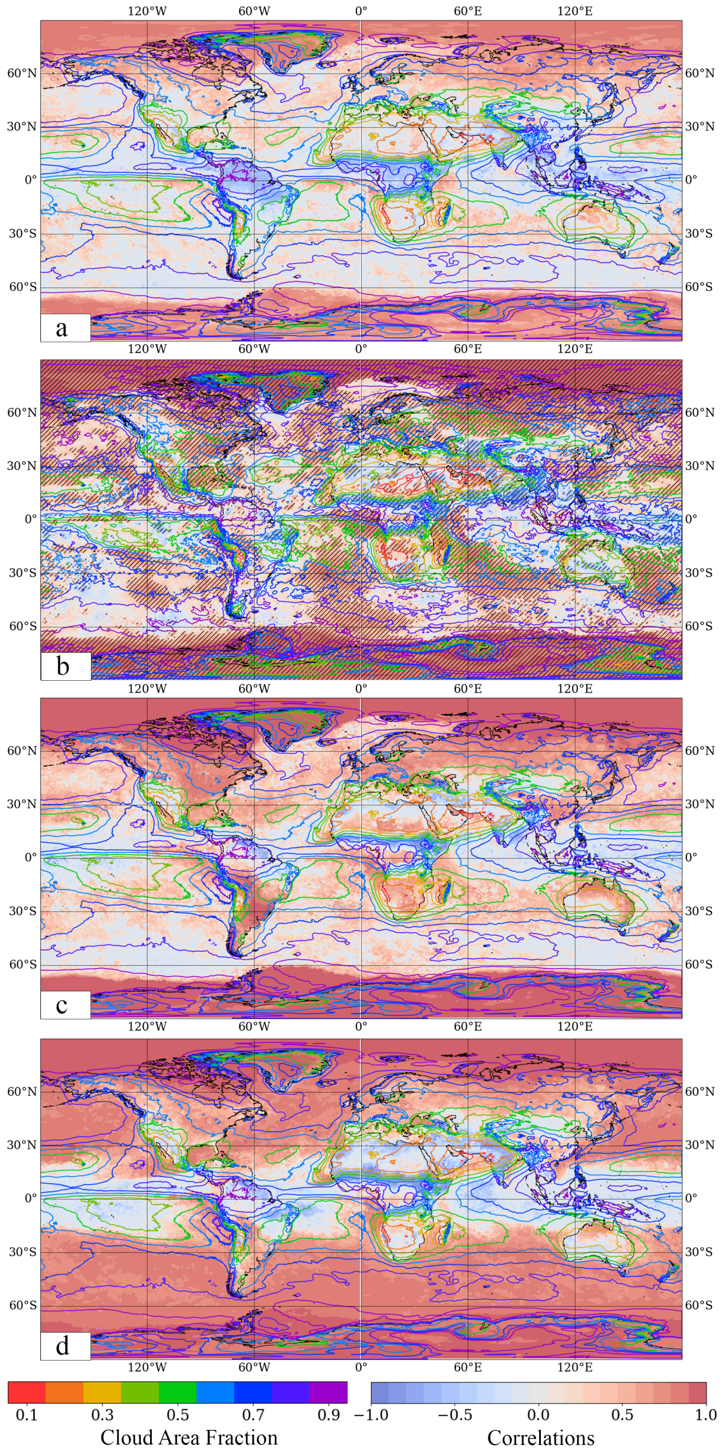

Figure S1. Correlations between – (a) daily T_{max} and CWV, (b) daily T_{max} and q_{sfc} for May 2016, (c) daily T_{avg} and q_{sfc}, and (d) daily $T_{2m,max}$ and q_{sfc}. All data from ERA5. All coefficients are multi-year modes for May 2001 to 2020 (as in Fig. 1), except panel b which shows coefficients for May 2016. Contour lines represent cloud cover averaged over the corresponding period. Correlations significant at the 95% confidence level are hatched in panel b.

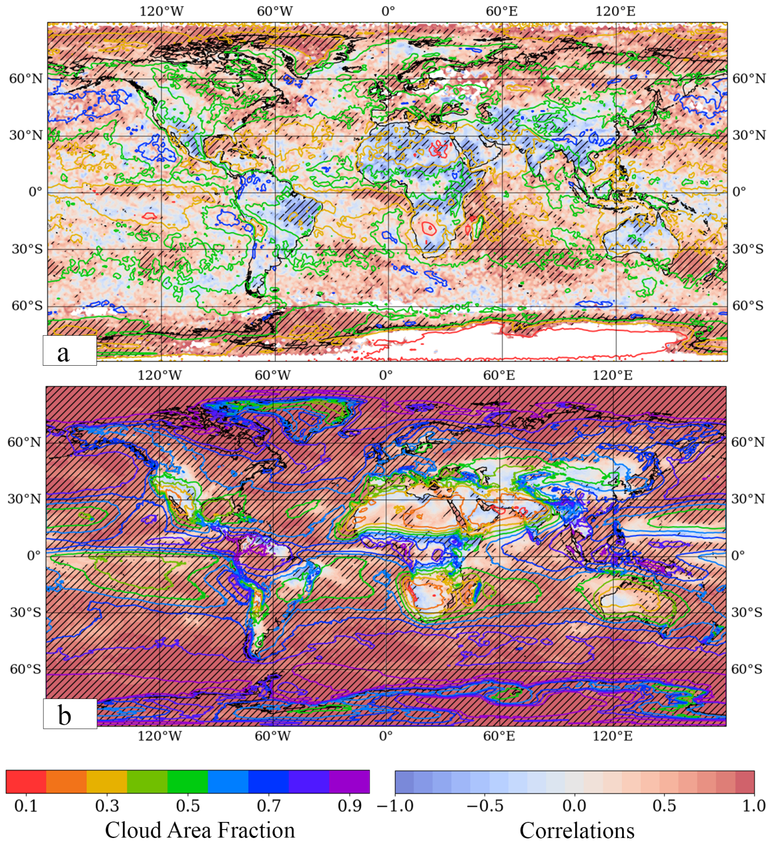

Figure S2. (a) Correlations between daily T_{max} and q_{sfc}, and daily averaged total cloud fraction from AIRS for May 2016, (b) Inter-annual correlations between monthly averaged T_{max} and q_{sfc} and corresponding daily averaged cloud cover for May 2001 to 2020 from ERA5. Correlations significant at the 95% confidence level are hatched.

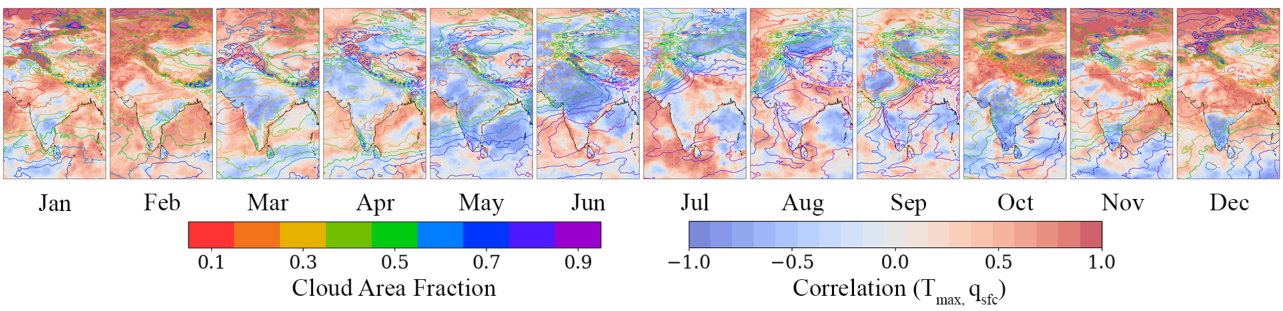

Figure S3. Grid scale correlations between daily T_{max} and q_{sfc} showing the seasonal pattern of IWVE over the Indian subcontinent for the year 2016.

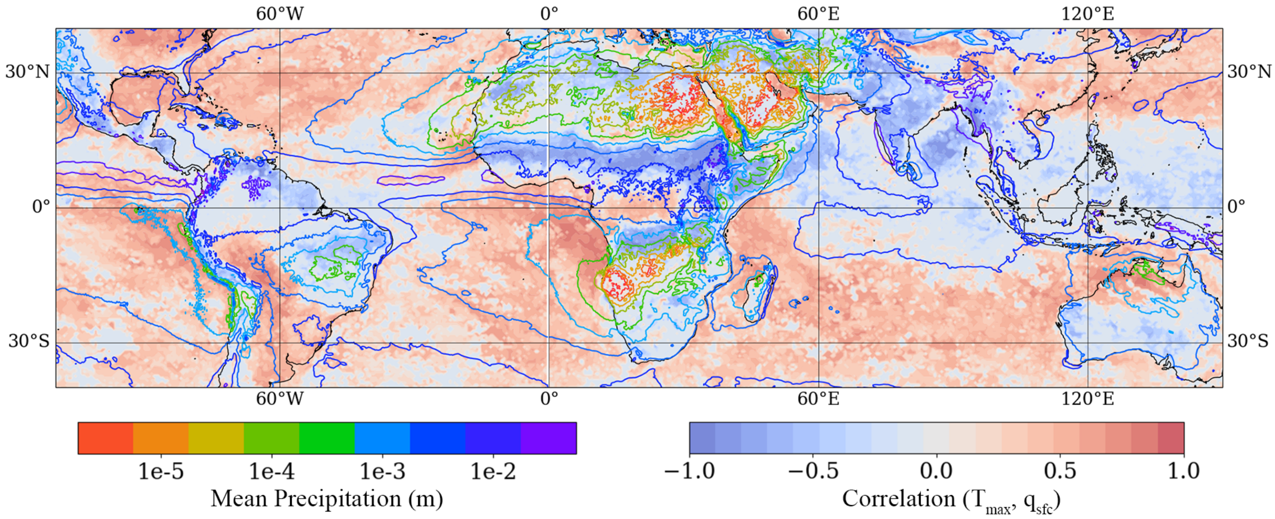

Figure S4. Same as Fig. 1 b but line contours show ERA5 precipitation averaged in May 2001 to 2020, instead of cloud fraction.

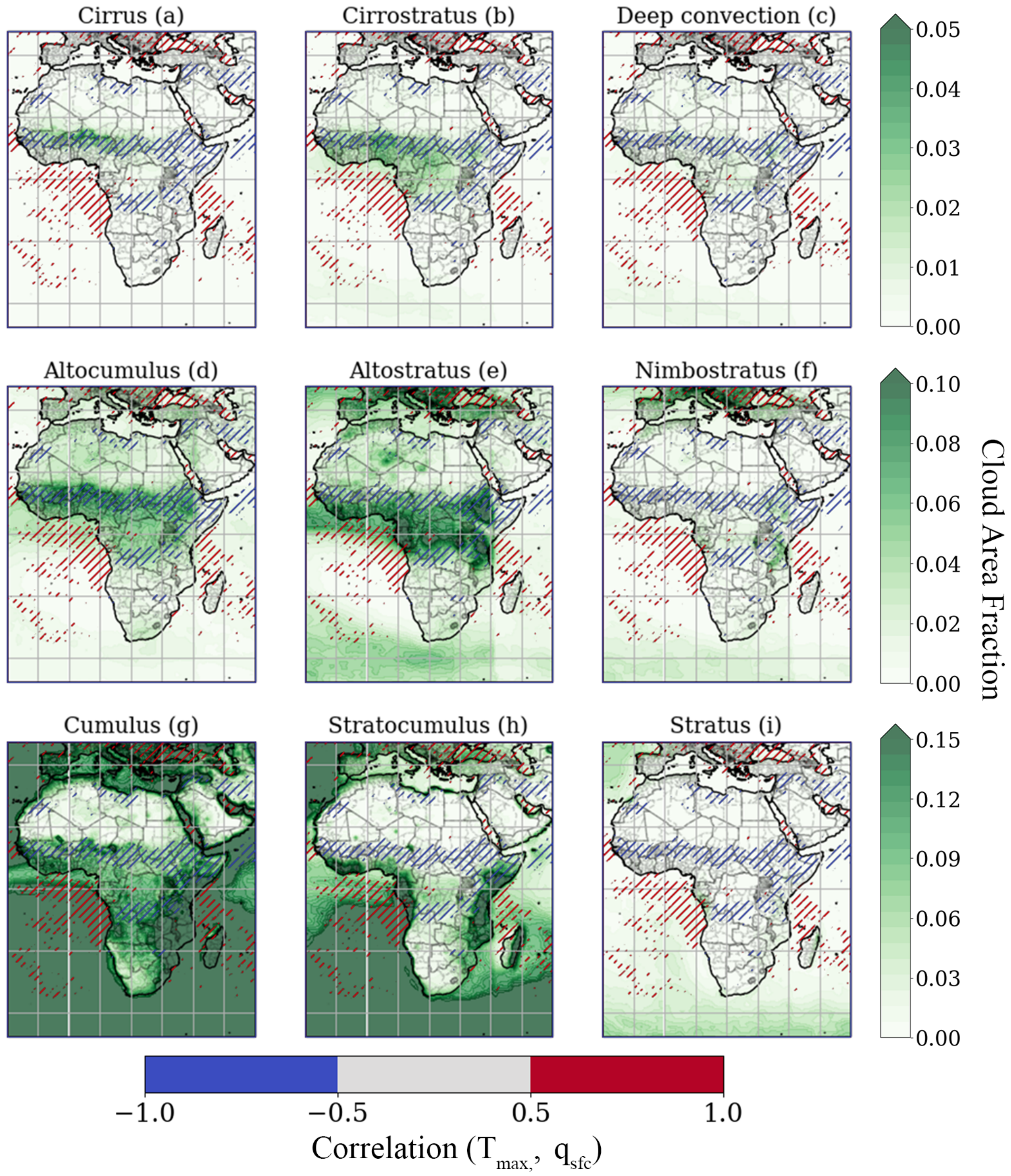

Figure S5. May cloud fraction averaged between 2001 and 2020 derived from CERES Cld-TypHist 1°x1° monthly data. Panels are arranged with highest clouds at the top and lowest clouds at the bottom. Optical depth increases from left to right. (a) Cirrus, (b) Cirrostratus, (c) Deep Convective clouds (d) Altocumulus, (e) Altostratus and (f) Nimbostratus, (g) Cumulus, (h) Stratocumulus and (i) Stratus. The blue and red hatching show regions with IWVE correlations between -1 to -0.5 and 0.5 to 1 respectively from Fig. 1b.

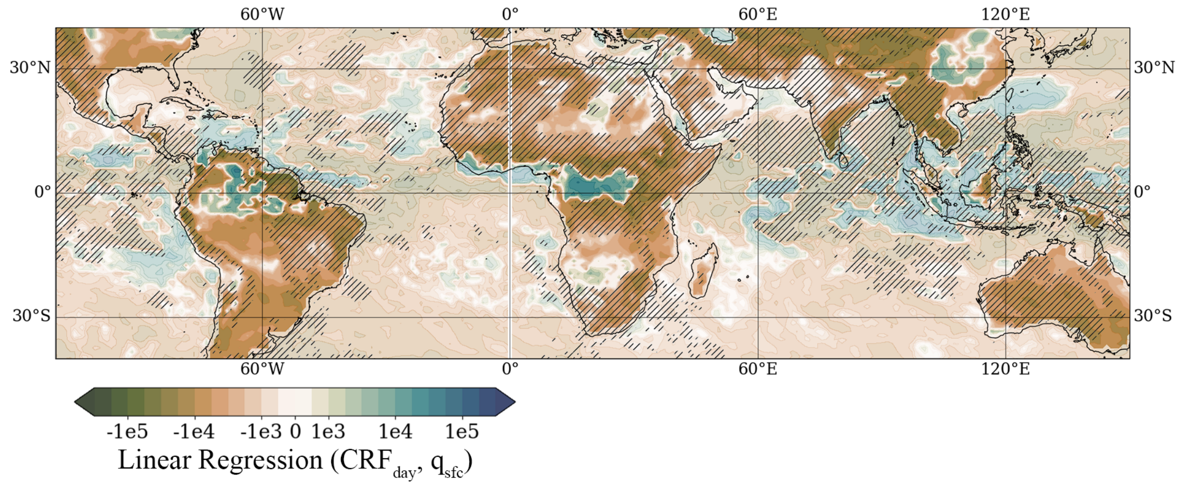

Figure S6. Same as Fig. 6 but with daily average *CRF* from CERES SYN1deg daily scale data for May 2016. Hatching shows all regions with negative IWVE correlations. Data obtained from ERA5.

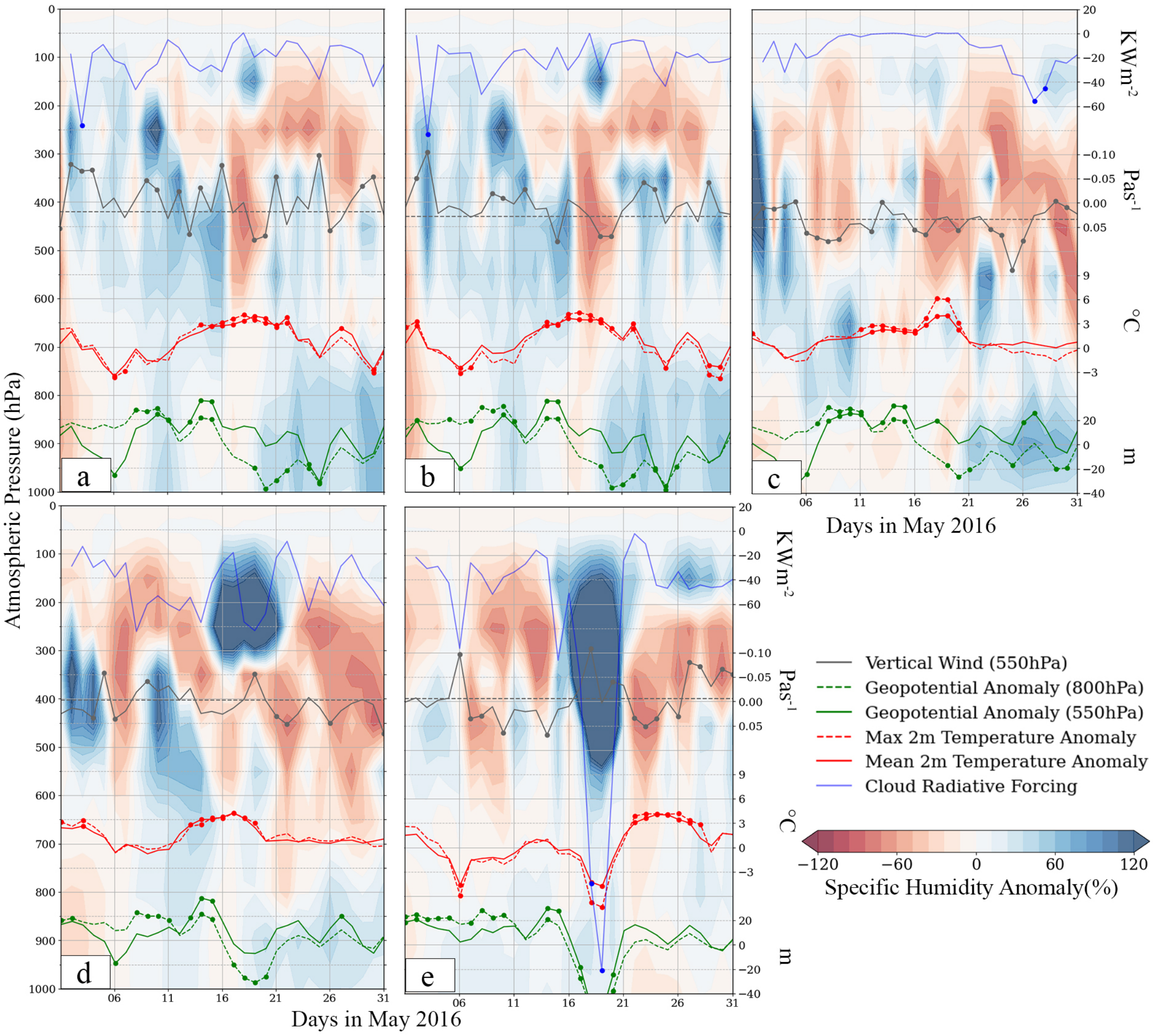

Figure S7. Same as Figure 8 but for (a) Datia, Madhya Pradesh (b) Lucknow, Uttar Pradesh, (c) Radhanpur, Gujarat, (d) Patoda, Maharashtra, and (e) Dachepalli, Andhra Pradesh.